10-31-1993

Far infrared fourier transform spectroscopy using ring interferometer

Changqing Qiu
New Jersey Institute of Technology

Copyright Warning & Restrictions

The copyright law of the United States (Title 17, United States Code) governs the making of photocopies or other reproductions of copyrighted material.

Under certain conditions specified in the law, libraries and archives are authorized to furnish a photocopy or other reproduction. One of these specified conditions is that the photocopy or reproduction is not to be "used for any purpose other than private study, scholarship, or research." If a, user makes a request for, or later uses, a photocopy or reproduction for purposes in excess of "fair use" that user may be liable for copyright infringement,

This institution reserves the right to refuse to accept a copying order if, in its judgment, fulfillment of the order would involve violation of copyright law.

Please Note: The author retains the copyright while the New Jersey Institute of Technology reserves the right to distribute this thesis or dissertation

Printing note: If you do not wish to print this page, then select "Pages from: first page # to: last page #" on the print dialog screen

ABSTRACT

Far Infrared Fourier Transform Spectroscopy Using Ring Interferometer

by
Changqing Qiu

A circular mirror interferometer named ring interferometer, which was designed by Dr. K.D. Möller, was built and set up for far-infrared Fourier transform spectroscopy. The ring interferometer has ten circular mirrors with the same area. By applying Fraunhofer diffraction theory, the calculation shows that the ring interferometer will have large diffraction angle range compared with lamellar grating interferometer which has rectangular mirrors with same width. Therefore the ring interferometer will be more efficient than lamellar grating in far-infrared spectroscopy. The experimental results show that this ring interferometer will work as expected.

In addition, a "home made" helium cooled detector was used in the experiment. A data acquisition and control system based on the WB-31 white box was also set-up and worked well. The Fourier transform spectroscopy was briefly reviewed in the thesis.

FAR INFRARED FOURIER TRANSFORM SPECTROSCOPY USING RING INTERFEROMETER

by
Changqing Qiu

A Thesis
Submitted to the Faculty of
New Jersey Institute of Technology
in Partial Fulfillment of the Requirements for the Degree of
Master of Science in Applied Physics

Department of Physics

October 1993

APPROVAL PAGE

Far Infrared Fourier Transform Spectroscopy Using Ring Interferometer

Changqing Qiu

Dr. Ken K. Chin, Thesis Adviser
Professor of Physics, NJIT — Date

Dr. K.D. Möller, Co-Thesis Adviser and Committee Member
Adjunct Research Professor in Applied Physics, NJIT — Date

Dr. John C. Hensel, Committee Member
Distinguished Research Professor in Applied Physics, NJIT — Date

BIOGRAPHICAL SKETCH

Author: Changqing Qiu

Degree: Master of Science in Applied Physics

Date: October 1993

Date of Birth:

Place of Birth:

Undergraduate and Graduate Education:

- Master of Science in Applied Physics,
  New Jersey Institute of Technology, Newark, NJ, 1993

- Bachelor of Science in Physics
  University of Science and Technology of China, Hefei, China, 1983

Major: Applied Physics

This thesis is dedicated to
my parents

ACKNOWLEDGMENT

The author wishes to express his sincere gratitude to his supervisor, professor Ken K. Chin, for his guidance, support and encouragement throughout this research.

Special thanks to Dr. K.D. Möller, the designer of ring interferometer. The thesis work would not complete without his idea, his experience, his help and guidance.

The author is grateful to professor John C. Hensel for helping establish the vacuum system and serving as committee member.

The author appreciates Mr. Cuono Anthony and Ramirez Herminio of physics Laboratory for their helping in mechanical machining work and Mr. Ganming Qin for his helping and suggestion in data acquisition and control system.

Finally , the author likes to thank all his friends in the Physics department for their kindness and supports.

TABLE OF CONTENTS

Chapter **Page**

LIST OF FIGURES

CHAPTER 1

INTRODUCTION

1.1 Far-Infrared Radiation

Far-infrared waves lie in the spectral region between wavelengths of 50 and 1000 μm, or from 200 to 10 cm^{-1} in wave numbers. The position of these waves in the spectrum is shown in Figure 1. As a part of the infrared spectrum, far-infrared radiation is fundamentally the same as any other electromagnetic waves. Thus the process of generation, transmission and detection of far-infrared radiation can be always treated with basic principles -- the Maxwell's equations of electrodynamics and the Schrödinger's equation of quantum descriptions. But with the longer wavelength, the techniques of far-infrared will be different from near or medium infrared mainly due to various transmission properties of materials and the reduced intensity of available radiation.

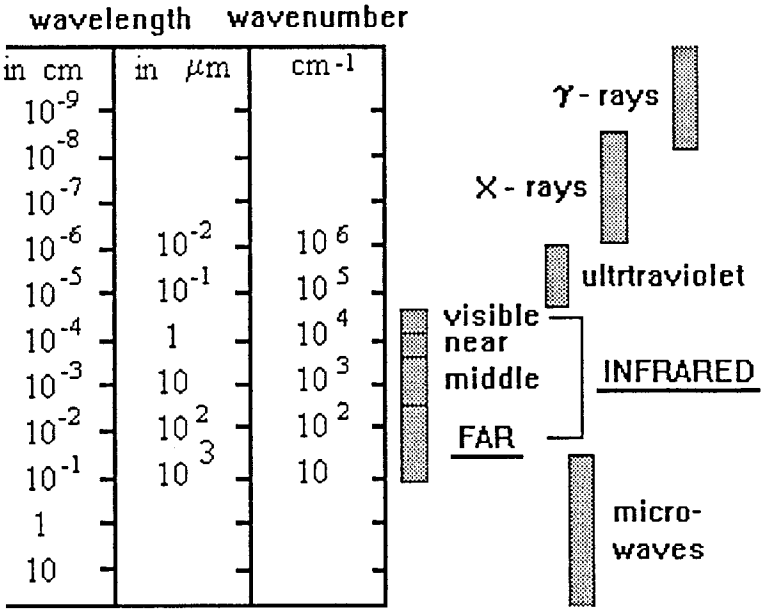

Figure 1 Electromagnetic spectrum

Historically, the development of the far-infrared has been handicapped by the difficulties of generators and the limitations of detectors. Toward longer wavelength, blackbody emission decreases rapidly according to Planck's radiation law. From Rayleigh-Jeans approximation to the Planck expression

$$B(\nu)d\nu = 2\pi ckT\nu^2 d\nu,$$

where $B(\nu)$ is energy distribution function, k is Boltzmann constant and ν is wavenumber, the emitted power in a wavenumber interval of fixed width decreases quadratically with decreasing wavenumber or increasing wavelength. On the other hand, due to the small energy ($E = h\nu$) of far-infrared photons, detectors with highest possible sensitivity are required. Given only weak sources and relatively insensitive detectors, far-infrared spectroscopists are forced to make an as efficient use of the available radiation energy as possible. In this respect, many new methods have offered to improve over conventional spectrometers. Here, we are going to introduce a new method-- the ring interferometer.

1.2 Spectra in Far-Infrared

The energies of far-infrared photons correspond to thermal energies at temperatures ranging from a few Kelvin to slightly above room temperature. Accordingly, the kind of transitions that can be studied in this spectral region have to do with rather weak forces or comparatively large masses ($\omega = \sqrt{k/m}$). The vibration of atoms within a molecule gives rise mainly to near-infrared frequencies, while the rotation and some other motion of molecules can be studied in the far infrared. The effects of the motions of molecules as individual particles in gases and liquids, as well collective motions in crystals as, also appear in this region. Resonant behavior of charged particles in gaseous plasmas, semiconductors, and metals can be observed at sub millimeter frequencies.

The far-infrared region is of interest to astronomy in connection with the cosmic background radiation, the existence of strong sources of radio and sub millimeter wave emission, and the presence of various molecular species in interstellar space. Besides, the possibility of realizing high-capacity communication links with sub millimeter waves also requires the study of atmospheric transmission properties in this region.

1.3 Far-Infrared Spectroscopy

The principles of far-infrared spectroscopy[1-4] remain the same as those in infrared spectroscopy[5]. The techniques used to explore this region have been developed by extending conventional infrared or microwave methods. As in the case of any spectroscopy, the two main problems of far-infrared spectroscopy still are:

(1) to pass as much radiation as possible through the dispersive system,

(2) to reject adequately unwanted short-wave radiation.

The spectrometer used in far-infrared spectroscopy can be classified into two main groups--prism and grating spectrometers on the one hand and various interferometric devices such as Fabry-Perot interferometers, Michelson interferometers, and interference modulators on the other.

As we know every monochromator or spectrometer can be evaluated by two fundamental characteristics:

(1) it's ability to resolve closely spaced spectral components which is characterized by the resolving power $R = \lambda/d\lambda = \nu/d\nu$ (λ = wavelength, ν = wavenumber)

(2) the luminosity or flux collected by the device from a source emitting unit power per unit area per unit wavelength interval.

In far-infrared spectroscopy, because of the lack of intense source in this region, the necessity that the instrument shall have high luminosity or ability to collect

radiation becomes relatively more important than at short wavelengths. This follows that the Fourier transform interferometer, with the Fellgett advantage that the whole spectral range of interest is incident upon the detector at one time, is vastly superiority over the grating spectrometer.

1.4 A Ring Interferometer

Nowadays the commonly used far-infrared spectrometers are Michelson and lamellar grating interferometers. The problem remains in them is their radiation dividers. For a Michelson interferometer, the beam splitter ideally has equal reflection and transmission coefficient, which is 0.5, at all frequencies. However, whether obtained by dielectric reflection from a film or from a wire screen, the ratio of reflection and transmission shows a marked frequency dependence and hence loss of efficiency. Lamellar grating interference modulator divided radiation wavefront instead wave amplitude by beam splitter, is more efficient in long wavelength. But due to diffraction on the modulator, it has a low frequency limit around 100 cm^{-1}.

For seeking an interferometer which is more efficient and can be used in whole far-infrared region, Dr. K.D. Möller[1,6-8] invented the circular mirror interferometer named ring interferometer. Instead of using same width rectangular mirrors in lamellar grating, ring interferometer use same area circular mirrors to modulate the radiation. The calculations show the angular distribution of light of destructive interference to be at a large range of angles for the circular reflectors in contrast to a narrow range for the rectangular reflectors. Therefore, the ring interferometer will have a higher efficiency for fringe production over a larger spectral range for the same area times solid angle used at source or detector than a wavefront dividing interferometer using rectangular reflectors.

1.5 The Objective of the Thesis

Represent ring interferometer as a more efficient Fourier transform interferometer for far-infrared region. Set up the optical system based on ring interferometer which has ten reflection mirrors. Testing the property of ring modulator. Use experimental results to examine the diffraction pattern derived from Fraunhofer diffraction theory.

CHAPTER 2

FOURIER TRANSFORM SPECTROSCOPY

2.1 Introduction

The science of Fourier transform spectroscopy[9] was initiated in 1880 when Dr. Albert A. Michelson invented the interferometer and was used in the far-infrared by Rubens and Wood in 1911 for investigations of the radiation emitted by a Welsbach mantle[10]. Figure 2 shows a Michelson-type two beam interferometer. The light from the source is divided by the beam splitter into beam I and II. Each beam is reflected at the mirrors I and II, respectively, and divided again at the beam splitter. with changing the position of one mirror, the overlap parts of beam I and II can be recorded as a interferogram -- the output for the entire spectral range as a function of the path difference. The spectrum can be yield by Fourier transform analysis. This kind technique which records information about all spectral intervals simultaneously is also called multiplex spectrometry.

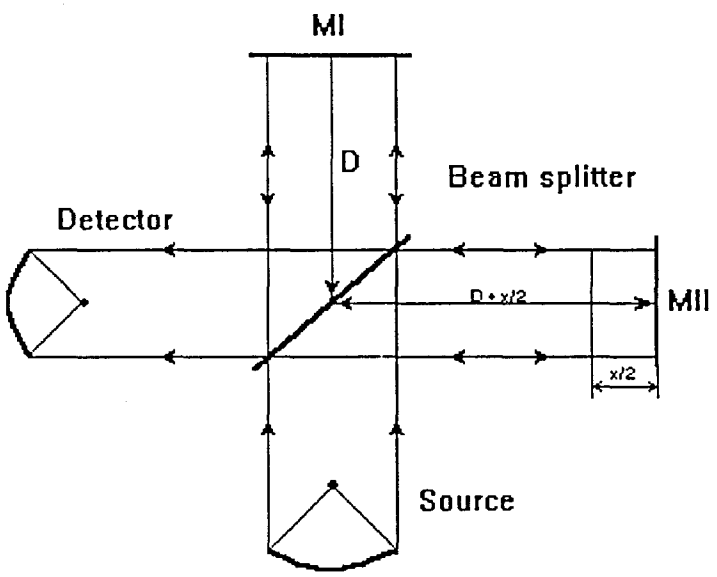

Figure 2 Optical schematic of a Michelson interferometer

Basically, the advantage of Fourier transform spectroscopy arise from two major concepts known as the Jacquinot and Fellgett advantages. In 1948 Jacquinot and Dufour pointed out that in contrast with monochromator that incorporates entrance and exit slits, Fourier Transform spectrometer has no slits. Therefore, the power transmission of the Fourier Transform Spectroscopy is grater than a grating spectrometer operating at comparable resolution. Consequently there can be much greater energy transmittance, and this is most important with weak incoherent sources in the far-infrared.

The multiplex or Fellgett principle can be explained as follows: Suppose one is interested in measuring a broad spectrum between the wave number ν_1 and ν_2 with a resolution $\delta\nu$. The number of spectral elements M in the broad band is then

$$M = (\nu_2 - \nu_1) / \delta\nu \equiv (\Delta\nu) / \delta\nu. \qquad (2.1)$$

If a grating or prism instrument is being used, each small band of width $\delta\nu$ can be observed for a time T/M, where T is the total time required for a scan from ν_1 to ν_2. The integrated signal received in a small band $\delta\nu$ is proportional to T/M. For an interferometer, because it detects the broad band $\nu_2 - \nu_1$ with resolution $\delta\nu$ at same time, the integrated signal in a small band $\delta\nu$ is proportional to T. If the noise is random and independent of the signal level, the signal-to-noise ratio S/N would be:

For grating $$(S/N)_G \propto (T/M)^{1/2}; \qquad (2.3)$$

For interferometer $$(S/N)_I \propto T^{1/2}. \qquad (2.3)$$

Therefore $$\frac{(S/N)_I}{(S/N)_G} = M^{1/2}. \qquad (2.4)$$

Since M is the number of spectral elements of width $\delta\nu$ in the broad band $\Delta\nu$, equation(2.4) predicts that the interferometer has a much higher signal-to-noise ratio than the grating or prism instruments.

2.2 Interferogram Function and Fourier Transformation

From Maxwell equations we can obtain plane wave solution as

$$u(x,t) = A\cos 2\pi(x/\lambda - t/\tau) \tag{2.5}$$

This is a transverse wave vibrating perpendicular to the x direction, having amplitude A, wavelength λ and period τ. The superposition of two waves with different path x_1 and x_2 will be

$$u = 2A\cos\left[2\pi(\delta/2)/\lambda\right]\left\{\cos\left[2\pi(x_1/\lambda - t/\tau) - 2\pi(\delta/2)/\lambda\right]\right\} \tag{2.6}$$

where $\delta = x_2 - x_1$ is the optical path difference. Therefore the intensity is

$$I = \left\{2A\cos\left[2\pi(\delta/2)/\lambda\right]\right\}^2\left\{\cos\left[2\pi(x_1/\lambda - t/\tau) - 2\pi(\delta/2)/\lambda\right]\right\}^2 \tag{2.7}$$

Only the second factor depends on time. Since the oscillation of the light is very fast, we assume that the detector may only register its average value, so we get

$$I = \left\{2A\cos\left[2\pi(\delta/2)/\lambda\right]\right\}^2. \tag{2.8}$$

That is, the intensity of the superposition of two space-time dependent harmonic waves depend only on the optical path difference δ. The interferogram and its Fourier transformation--the frequency spectrum is shown in Figure 3.

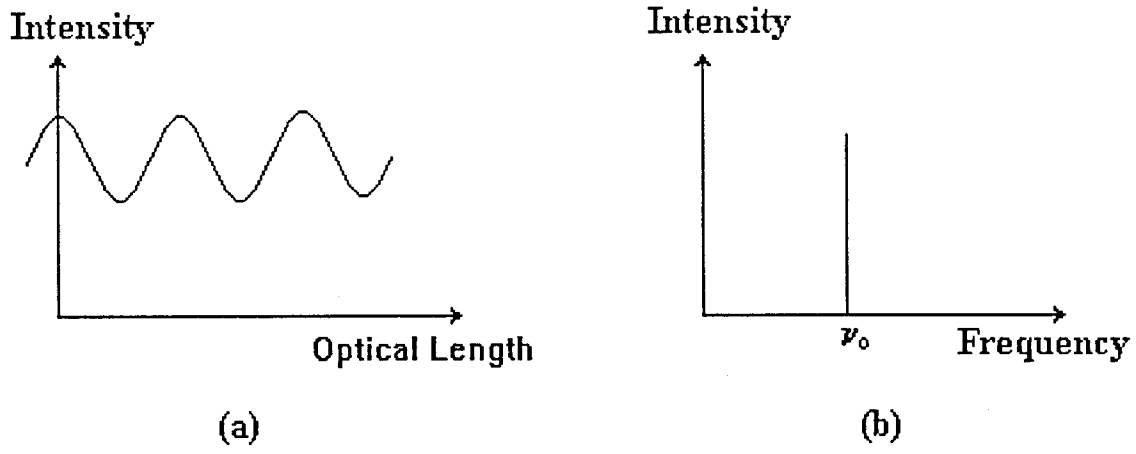

Figure 3 (a) Interferogram of an incident monochromatic wave. (b) The Fourier transform is a single frequency.

Considering the incident wave containing p waves of amplitude A_j and wavelength λ_j, by using notation y as optical path and writing $\nu_j = 1 / \lambda_j$ as frequency, the superposition of p waves on the screen site can be directly obtained from equation (2.8) as

$$I(y) = \sum_{j=1}^{p} 2A_j^2 \left[1 + \cos\left(2\pi\nu_j y\right)\right]. \tag{2.9}$$

Here the fundamental equation used is

$$2\cos^2 x = 1 + \cos 2x$$

For continuous frequency distribution from $\nu = 0$ to $\nu = \infty$, equation (2.9) become

$$J(y) = 2\int_0^\infty G(\nu)\left[1 + \cos 2\pi\nu y\right]. \tag{2.10}$$

For specific case of y = 0, we have

$$J(0) = 4\int_0^\infty G(\nu)d\nu. \tag{2.11}$$

In the Fourier integrals we need for ν and y the range from $-\infty$ to ∞. We formally extend the frequency range by assuming that $G(\nu)$ is symmetric around $\nu = 0$ and therefore that $G(-\nu) = G(\nu)$. So from equation (2.11), we then have

$$J(0) = 2\int_{-\infty}^{\infty} G(\nu)d\nu \tag{2.12}$$

and for equation (2.10) with the expansion of the cos-function as exponential

$$J(y) = \int_{-\infty}^{\infty} G(\nu)\left(1 + e^{i2\pi\nu y}\right)d\nu. \tag{2-13}$$

Introduction of equation (2.12) into equation (2.13) gives us

$$J(y) = \frac{1}{2}J(0) + \int_{-\infty}^{\infty} G(\nu)e^{i2\pi\nu y}d\nu. \tag{2-14}$$

Rewrite equation (2.14), we get the interferogram function S(y) as

$$S(y) = J(y) - \frac{1}{2}J(0) = \int_{-\infty}^{\infty} G(\nu) e^{i2\pi\nu y} d\nu . \qquad (2\text{-}15)$$

Using Fourier transform analysis, the spectrum G(ν) can be obtained by inverse Fourier transformation integral

$$G(\nu) = \int_{-\infty}^{\infty} S(y) e^{i2\pi\nu y} dy . \qquad (2.16)$$

The integration is over the space coordinate y, and wave number ν appears as a parameter. Equation (2.16) is the basic relation of Fourier transform spectroscopy. As path difference of a two-beam interferometer is changed progressively, the output is registered with a detector. The Fourier cosine transform of recorded interferogram is calculated to yield the spectrum G(ν).

2.3 Resolving Power and Apodization

As mentioned before, the resolving power in all spectrometers is determined by the maximum path difference between two interfering waves. In the case of the two-beam interferometer, the movable reflector can be displaced only over a limited range -L to L, where L = y_{max}, and this determines the resolving power. By restricting the range on the limits of integration, Equation (2.16) gives the approximate spectrum

$$G'(\nu) = \int_{-L}^{L} S(y) \exp(i2\pi\nu y) dy \qquad (2.17)$$

To find the resolving power, consider monochromatic incident radiation of wavenumber ν_0 and unit intensity, as Figure 3 shown, $G(\nu) = \delta(\nu - \nu_0)$, δ being the Dirac delta function. The interferogram function is then

$$S(y) = 2\cos 2\pi\nu_0 y,$$

and the spectrum determined is

$$G'(\nu) = 2\int_{-L}^{L} \cos 2\pi\nu_0 y \cos 2\pi\nu y dy$$

and the integration result will be

$$G'(\nu)=\left[\frac{\sin 2\pi(\nu-\nu_0)L}{2\pi(\nu-\nu_0)L}+\frac{\sin 2\pi(\nu+\nu_0)L}{2\pi(\nu+\nu_0)L}\right]2L\,. \tag{2.18}$$

In practice, the path difference between the two interfering beams is varied over many wavelengths, so for all frequencies of interest $\nu L \gg 1$, and the second term of Equation (2.18) is negligibly small. The first part

$$\frac{\sin 2\pi(\nu-\nu_0)L}{2\pi(\nu-\nu_0)L} \tag{2.19}$$

is the function recorded at the output when an infinitely sharp spectral line of frequency ν_0 illuminates the interferometer, and it plays an analogous role in determine the resolution.

But from the point view of resolution, Equation (2.19) is not entirely satisfactory because the secondary maxim are so large that they would tend to hide weak lines in the vicinity of a strong line. It is desirable to reduce them considerably, and this can be done by a process called apodization. This process consists of introducing an additional function A(y) so that the truncated integral of Equation (2.16) takes the form

$$G(\nu)=\int_{-L}^{L}S(y)A(y)\cos 2\pi\nu y dy \tag{2.20}$$

where A(y) is the apodization function.

The Rayleigh criterion that two spectral lines are resolved when their diffraction patterns are displaced by the separation between the principal maximum and the first minimum gives the resolving power for the unapodized case [equation (2.19)]:

$$R = \nu / d\nu = \nu L = L / \lambda \tag{2.21}$$

This condition, that two frequencies are resolved if $L d\nu > 1$, means that maximum

displacement of the movable reflecting element of the interferometer must produce a differential phase shift of 2π or more between the two frequencies. See Figure 4.

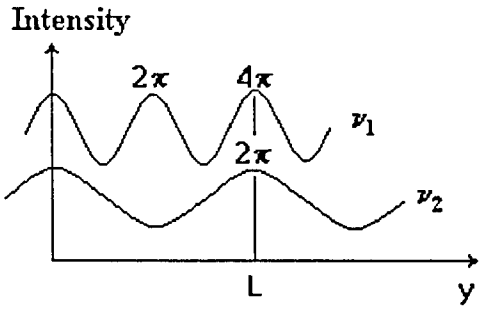

Figure 4 Two frequency will be resolved with phase shift of 2π

Apodization can decrease the secondary maxim. However, the price paid for this improvement is that the width of the central peak widens, this degrading the resolving power.

2.4 Sampling The Interferogram

In a computer sampling system, the basic equation (2.16) must be modified into discrete form

$$G(K\Delta\nu) = \sum_{I=-N/2}^{N/2} S(I\Delta y)\exp[i2\pi(K\Delta\nu)(I\Delta y)]\Delta y \ . \qquad (2.22)$$

That is, the infinite limits of integration must be replaced by the finite limit of mirror movement Δy and the integration is replaced by a sum over finite increments. Here, the relation between the maximum mirror movement and the number N is $L = N\Delta y / 2$. In Fast Fourier Analysis, there must have $N = 2^M$, where M is an integer.

To decide how far apart the sampling points in the interferogram can be, or simply saying, what is the maximum value of Δy, the methods of information theory need to be applied. But the conclusion can be easily understood by referring

to Figure 5. For a certain frequency ν_0, the correspond cosine should be sampled at least twice per period. If the highest frequency which we shall encounter in the spectrum is ν_{max}, by using this twice-per-cycle criterion, we can get the maximum value of Δy at once from the argument of the cosine

$$\Delta y_{max} = \frac{1}{2}\lambda_{min} = \frac{1}{2\nu_{max}} . \tag{2.23}$$

Thus the frequency of sampling is determined by the highest spectral frequency present in the spectrum. The number of sampling points in the interferogram is then $2\nu_{max}L$. If we restrict the investigation to the frequency rang

$$\nu_{min} \leq \nu \leq \nu_{max},$$

a similar consideration as presented above yields the sampling interval

$$\Delta y_{max} = 1 / [\, 2(\nu_{max} - \nu_{min}) \,].$$

That is , by restricting the spectral region to a smaller bandpass, the sampling interval will be increased (fewer sampling points).

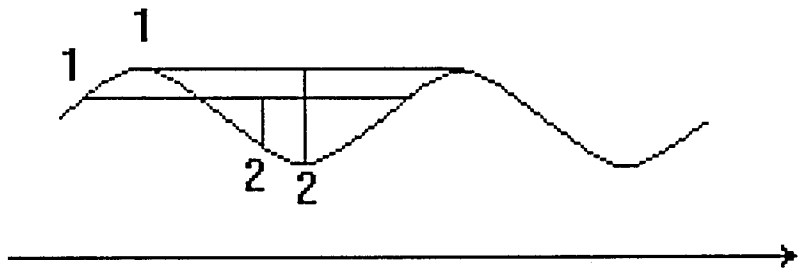

Figure 5 The cosine should be sampled at least twice per period.

CHAPTER 3

WAVEFRONT DIVIDING INTERFEROMETER

3.1 Lamellar Grating Interferometer

Another type of two-beam interferometer for Fourier Transform spectroscopy is the lamellar-grating interferometer, which was invented by Strong and his coworkers. In contrast to the amplitude division by beam splitter of the Michelson interferometer, the lamellar grating divide the wave front itself into two interfering parts. Figure 6 is the diagram of the lamellar grating interferometer. when wavefront proceeds to the modulator, it will divided such that one-half of the beam is reflected from the front facet or strip mirrors an one-half goes farther to back

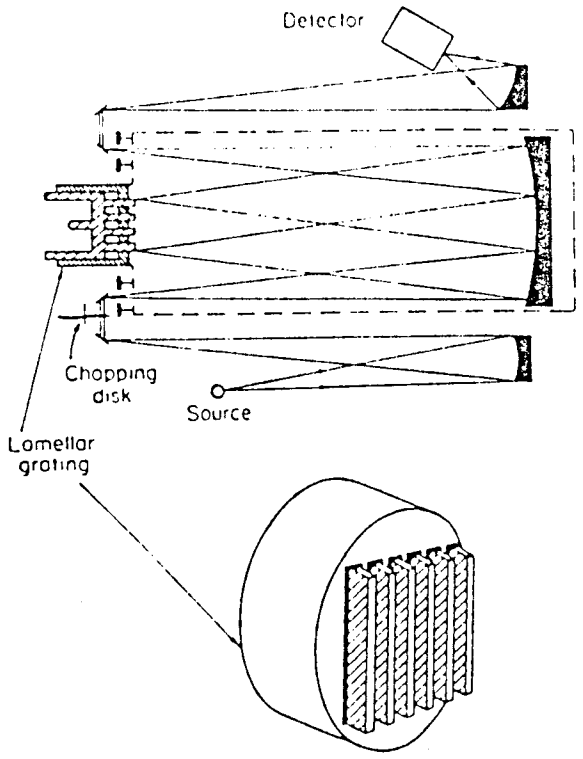

Figure 6 Diagram of the lamellar grating interferometer

facets before being reflected. If the back facets are a distance D behind the front facets, an optical path difference of 2D is introduced between the two parts of the wave. The collimated beams return to second large mirror and are focused on the detector.

From the scheme we see that there is no beam splitter in a lamellar grating interferometer, so it is more efficient than the Michelson interferometer. Figure 7 shows the efficiency of a lamellar grating interferometer and a Michelson interferometer using a metal screen and a Mylar film beam splitter[11]. Unfortunately, the high efficiency of the lamellar grating interferometer occurs at wave numbers below about $100cm^{-1}$, because of diffraction on the grating. Since this frequency limit and the complicated mechanical construction, the lamellar grating interferometer has not found as many applications in Fourier Transform Spectroscopy as the Michelson interferometer has. But in Far-Infrared region, we see that the wavefront dividing type interferometer will have some promising future.

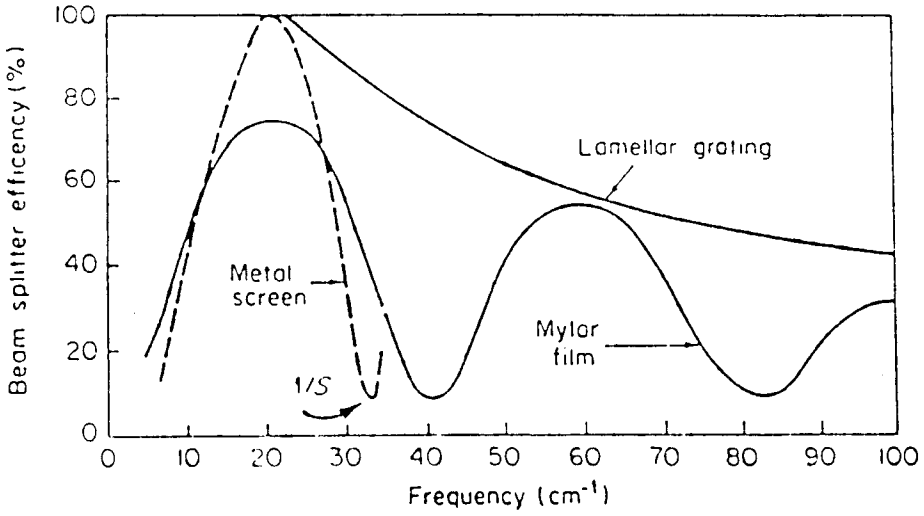

Figure 7 Efficiency of mylar, metal screen, and lamellar grating modulator as a function of wavenumber. The mylar is 0.003 in thick and the wire screen has ~ 250 lines per cm.

3.2 Diffraction on Wavefront Dividing Interferometer

A major problem encounted in the wavefront dividing interferometer like the lamellar grating is the diffraction on the grating. By applying scalar-Fraunhofer diffraction theory to the lamellar grating problem, the grating can be treated as two sets of mirrors--the front facets and the back facets. Each set of strip mirrors can be considered as a linear array of identical long, rectangular apertures. In reference 7, Dr. K.D. Möller calculated the Fraunhofer diffraction pattern for 2 to 4 mirrors. As an example, Figure 8 shows the diffraction pattern of two mirrors of width d, with optical path difference between one another of h=1/6, 2/6, ··· to 6/6 times wavelength λ. The normalized intensity is giving by the equation

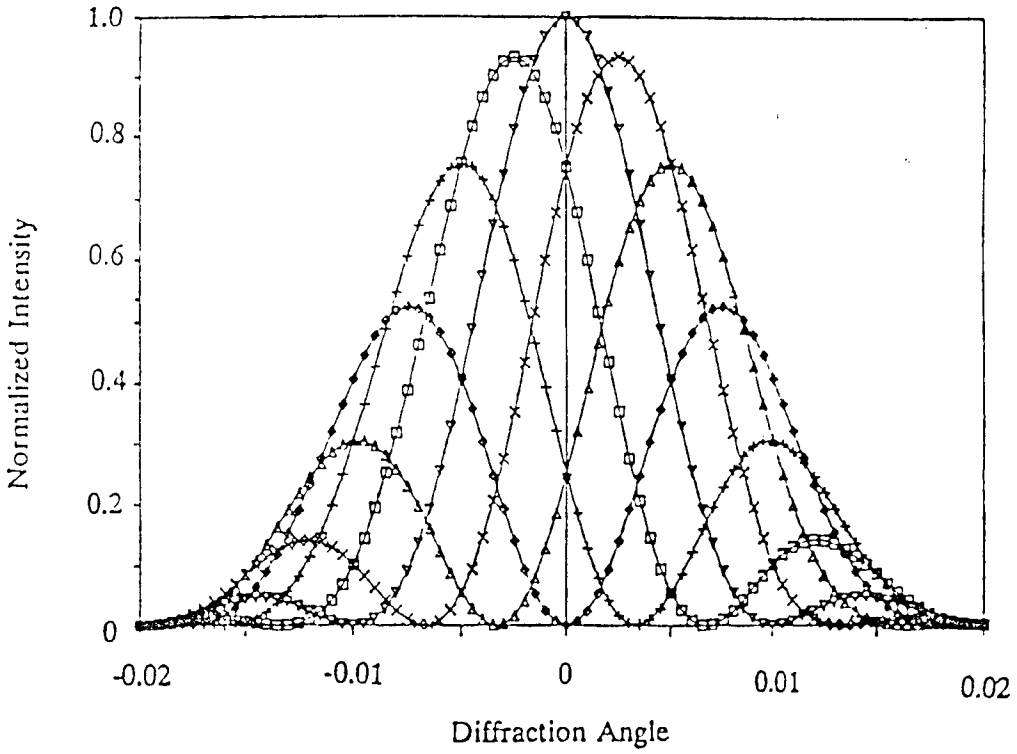

Figure 8 Diffraction pattern of two rectangular mirrors of width d. The optical path differences are ×, 1/6; Δ, 2/6; ◊, 3/6; +,4/6; □,5/6; ∇,6/6; of wavelength.

$$\frac{u^2}{u_0^2} = \left[\frac{\sin\left(\pi\frac{d}{\lambda}\sin\theta\right)}{\pi\frac{d}{\lambda}\sin\theta}\right]\cos^2\left(\pi\frac{d}{\lambda}\sin\theta+\frac{\varphi}{2}\right) \tag{3.1}$$

where $\varphi=2\pi h/\lambda$ is the phase difference between two mirrors. From the figure we see that with increasing displacement of the mirrors, the peak of the pattern moves to one side and comes back from the other side. When the center peak is at minimum, the side maxim are equally high. There is no location in a certain angle range for the diffraction pattern for different path differences.

For more mirrors, the situation is basically the same. Actually, the diffraction pattern of a lamellar grating in zeroth order is the same as the interference pattern required in Fourier transform spectroscopy. If one get only zeroth order pattern without high order, especially first order pattern, one get the optimum modulation of the interferogram. But as we know that the angle of the first order with respect to the direction of reflection (zeroth order) is determined by λ/a, where a is the width of the mirror. Considering a source with two wavelengths, the pattern for the shorter wavelength is narrower. If an aperture has been selected just to pass the light of constructive interference, then for a shorter wavelength some light of destructive interference will pass and reduce the efficiency of the interferometer. For the source with whole range of frequency, this means a certain fraction of the first order light will be detected. If this fraction is small enough, the interferogram may still be usable.

The diffraction on wavefront dividing type interferometer can not be avoided. What we can do is to arrive at diffraction pattern having the intensity corresponding to constructive interference at the center and the intensity corresponding to destructive interference as far away the center as possible.

3.3 Ring Interferometer

In his paper[8], Dr. K.D. Möller described his new instrument initially to use the spatially coherent properties of infrared synchrotron radiation which is about 1000 times bright than a conventional mercury source across the entire infrared region. The recent design is shown in Figure 9. The circular ring mirrors have same area, so that the width of Nth mirror is equal to $1/\sqrt{N}$ times the radius of the central part. The separate parts can be moved by step motor, so that it form a Fourier transform modulator.

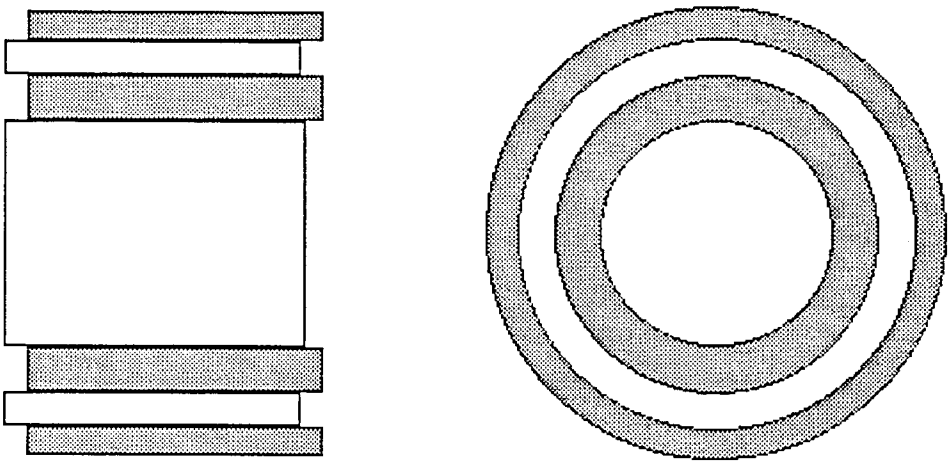

Figure 9 The schematic of ring interferometer

Obviously, this is also a kind of wave-front-dividing interferometer which does not need beam splitter. The design of the ring interferometer makes it possible to distribute the first order over a large area. First it distributes the light in two dimensions because the diffraction is two dimensional. Second the reflectors has different width so that the first order is not diffracted into one single angle, as we know that the angle of the first order with respect to the direction of reflection is around λ/d. We may see this by comparison with a set of reflectors having all the same width, see Figure 10.

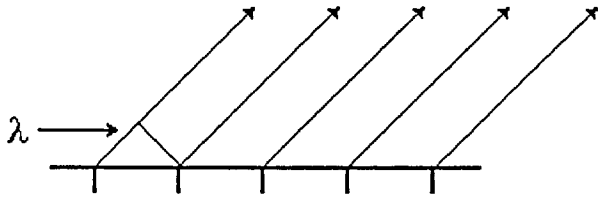

[a] The reflectors have equal width

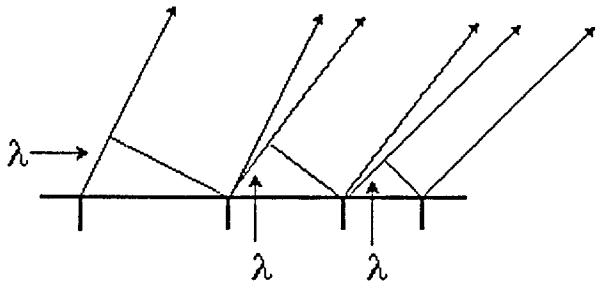

[b] The reflectors have unequal width

Figure 10 first order diffraction from mirror sets

For a broad band input, the highest frequency is now distributed not into a single angle as it is for the lamellar grating, but over an angle range, and similarly for all lower frequencies. If we may admit a certain fraction of the first order light on the detector, but still get an interferogram with sufficient modulation, we may use a much larger frequency range than is possible with the lamellar grating. So we see that the ring interferometer will be a more efficient wavefront dividing interferometer.

3.4 Diffraction on Ring Interferometer

By using notation a_1 as the radius, r and ϕ the coordinates of the circular aperture, R and φ the coordinates of the diffraction pattern (on the screen) and x the distance, the Fraunhofer amplitude diffraction pattern for a round aperture can be written as

$$u = u_0 \int_{-\pi}^{\pi} \int_{0}^{a_1} \exp\left[i2\pi \left(\frac{r}{\lambda} \frac{R}{x} \right) \cos(\varphi - \phi) \right] dr d\phi \,. \tag{3.2}$$

With the help of Bessel function of zeroth and first order, the result of the integration is

$$u\left(\frac{R}{x}\right) = u_0 2\pi a_1^2 \frac{J_1\left[2\pi\left(\frac{a_1}{\lambda}\frac{R}{x}\right)\right]}{2\pi\left(\frac{a_1}{\lambda}\frac{R}{x}\right)} \quad . \tag{3.3}$$

With the use of the notation

$$\left(\int a_n\right) = 2\pi a_1^2 \frac{J_1\left[2\pi\left(\frac{a_n}{\lambda}\frac{R}{x}\right)\right]}{2\pi\left(\frac{a_n}{\lambda}\frac{R}{x}\right)} \quad , \tag{3.4}$$

the Fraunhofer intensity diffraction pattern of a mirror of radius a_1 and a ring of outer radius of a_2 which equal to $\sqrt{2}$ times a_1, can be calculated as

$$\frac{u^2}{u_0^2} = 4\pi \sin^2\frac{\varphi}{2}\left[\left(\int a_1\right)^2 - \left(\int a_1\right)\left(\int a_2\right)\right] + \left(\int a_2\right)^2 \quad , \tag{3.5}$$

where φ is phase difference of the center mirror.

Figure 11 plotted the diffraction pattern of two circular mirror set [7]. The radius of the outer ring is the square root of the inner one. The intensity as function of the diffraction angle (R/X) is shown for the optical path differences -,1/6; -,2/6; ◊,3/6; +,4/6; □,5/6; -,6/6; of wavelength. Since the pattern is rotational symmetry, the intensity is plotted in the radial direction. The intensity is normalized to 1 at the center; and the radius of the center mirror to the wavelength is taken to be 25.

Compared with rectangular two mirrors shown in Figure 8, we see a better intensity distribution over the plane of the diffraction pattern. The intensity for destructive interference (3/6) is further removed from the center for the circular

mirrors than for the linear mirrors and note that the circular mirror pattern has plotted over a large angle range.

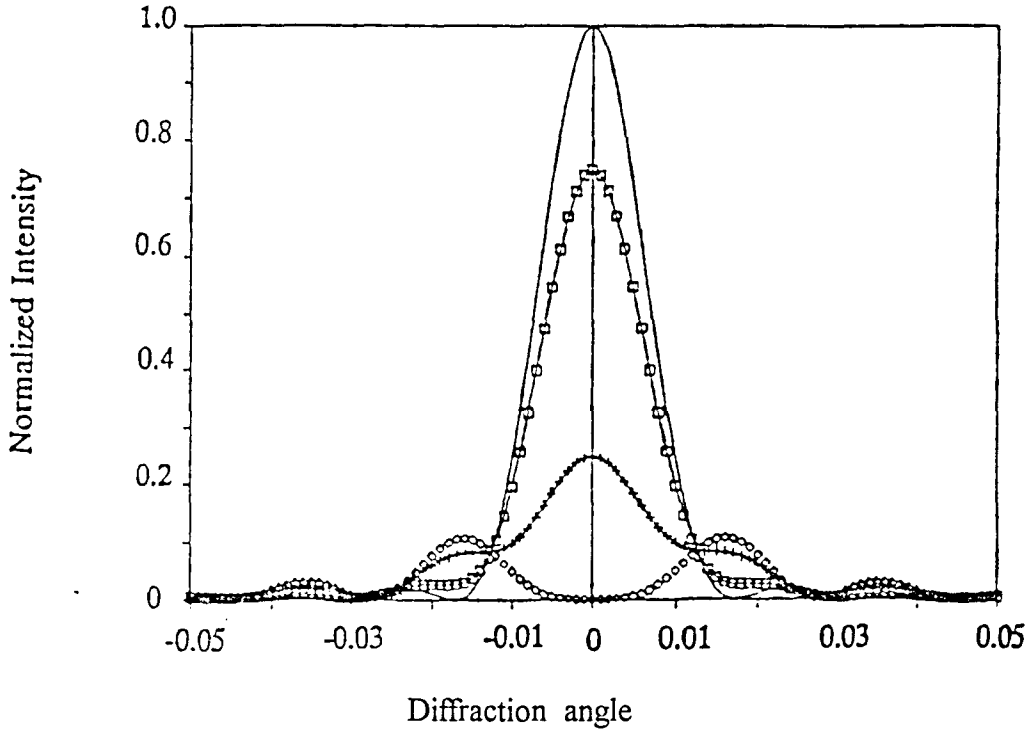

Figure 11 Diffraction pattern of two circular mirror set

For the ring interferometer which the radii of the mirrors and rings are $\sqrt{N}$ times the radius of the center mirror, the Fraunhofer diffraction pattern of the amplitude of N rings may be calculated as

$$u = u_0\left\{\left(\int a_1\right)\exp(i\varphi)+\left[\left(\int a_2\right)-\left(\int a_1\right)\right]+\left[\left(\int a_3\right)-\left(\int a_2\right)\right]\exp(i\varphi)\right.$$
$$\left.+\cdots+\left[\left(\int a_n\right)-\left(\int a_{n-1}\right)\right]\right\}. \qquad (3.6)$$

Assume n is even, the intensity of the diffraction can be obtained as

$$\frac{u^2}{u_0^2} = 4\sin^2\frac{\varphi}{2}\left(\sum\pm\int a_{n-1}\right)\left[\left(\sum\pm\int a_{n-1}\right)-\left(\int a_n\right)\right]+\left(\int a_n\right)^2. \qquad (3.7)$$

For constructive interference we have $\varphi = 0$ and obtain from equation (3.7)

$$\frac{u^2}{u_0^2} = \left(\int a_n\right)^2 \tag{3.8}$$

and for destructive interference, $\varphi = \pi$, we have

$$\frac{u^2}{u_0^2} = 4\left(\sum \pm \int a_{n-1}\right)\left[\left(\int \sum \pm \int a_{n-1}\right) - \left(\int a_n\right)\right] + \left(\int a_n\right)^2 . \tag{3.9}$$

In case of constructive interference, the intensity is represented by the diffraction pattern of a mirror-aperture of radius a_k, most of it is in the center.

In the case of destructive interference, the intensity is represented in a complicated way by a superposition of all the diffraction pattern produced by the reflecting area of radii from a_1 to a_k equal $\sqrt{N}a_1$ (unequal with of rings). At the center we have zero intensity since $q \rightarrow 0$ we have $J_1(q)/q = 1/2$, the exponential is -1 and the sum term is equal to a_1^2 (-n/2+n) canceling the last term which is equal to $a_1^2 n$.

From the calculation, one sees that for the circular mirrors the intensity corresponding to destructive interference is much more distributed over a large area and removed from the center compared to lamellar grating. This translates into a much larger modulation for shorter wavelength in the case of circular mirror interferometer. Since the intensity of black body and synchrotron radiation increases from the very long wave drastically to shorter wave length, the circular mirror interferometer is promising to be applicable over a large spectral region. A similar consideration applies to an extended source area.

CHAPTER 4

SPECTROMETER SET UP FOR RING INTERFEROMETER

4.1 Schematic of the Spectrometer

The optical layout and the experimental arrangement are schematically shown in Figure 12. The light from the mercury-arc lamp which is set in the light source chamber is focused by source mirror onto the entrance aperture of light pipe I. A chopper with frequency of 16 Hz is placed before the entrance of the light pipe to chop the light and produce the reference signal for the lockin amplifier at the same time. At the exit of light pipe I, a small flat mirror reflects the light to a large collimating mirror. The parallel light from this mirror is incident on the ring interferometer, is reflected and diffracted, and the light is focused onto the entrance opening of light pipe II. The exit of light pipe II is connected to the entrance light pipe of the detector.

All the components of the spectrometer are inside the vacuum chambers, because water vapor in the atmosphere has strong absorption to the far-infrared radiation and may be used for calibration of the spectrometer, the vacuum may be chosen to be a few Torr and calibration lines may be observed in absorption with a broad band light source. There is a provision in the sample tank to focus the light from the light pipe II (a shorter version) onto a sample cell, and after passing the cell it is focused with a second mirror at the entrance of the light pipe of the detector.

The ring interferometer has totally 10 facets made of aluminum alloy. The outer 5 facets are fixed on metal stand while inner 5 ones can be precisely moved by step motor. The radius of center mirror is 2.54 cm, so that the area of each mirror is 22 cm^2 and the total area is 220 cm^2.

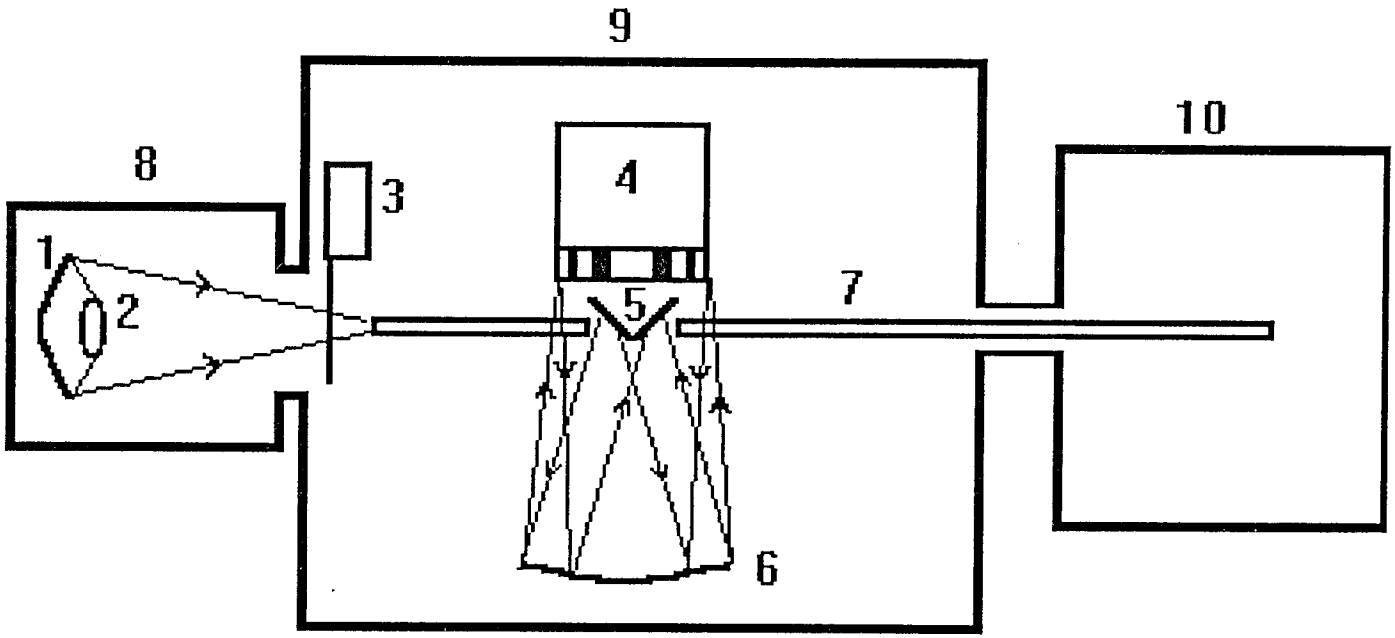

Figure 12 Spectrometer schematic of ring interferometer
1. Source mirror 2. Mercury arc lamp 3. Chopper 4. Ring interferometer 5. Small reflection mirror 6. Focusing mirror 7. Light pipe 8. Source tank 9. Spectrometer tank 10. Sample chamber

4.2 The light Source.

The most frequently used radiation sources in the far-infrared are the mercury-arc lamp and the globar (silicon carbide). Figure 13 shows the actual data of Plyler for the 50 to 170 cm^{-1} region[12], radiation energy is given in arbitrary units. We see that for frequencies smaller than 140 cm^{-1}, the mercury-arc lamp is more efficient in the far-infrared than the globar source.

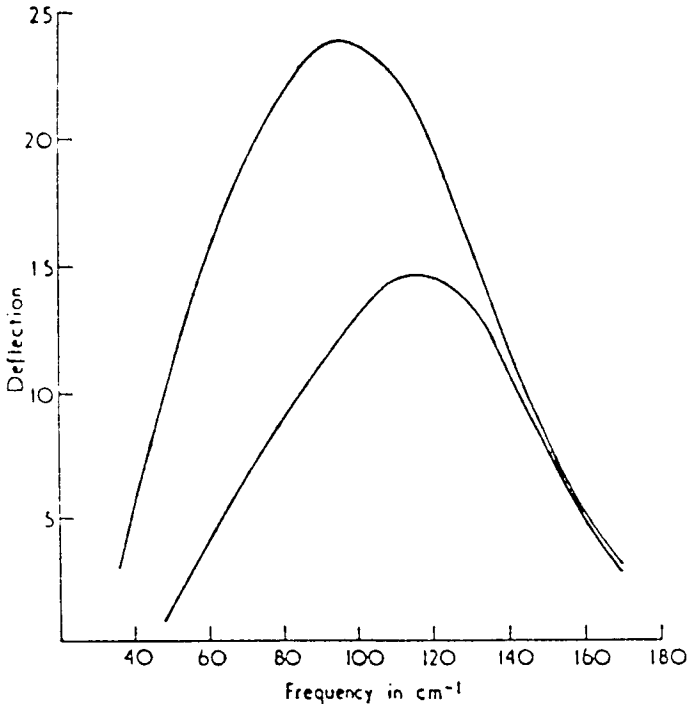

Figure 13 Radiant energy of a quartz-mercury lamp (upper curve) and a globar source (lower curve) from 50-170cm^{-1}

The source used with the interferometer is a 250 watts mercury lamp. The glass envelope of the Mercury lamp must be removed since glass is not transmissive in the far infrared. Figure 14 shows the fused quartz envelope of the lamp of 12.5 mm (1/2 inch) diameter. The outside of the tube is heated by the burning arc and emits light as a black body of about 1400°K. The arc inside the

tube emits mainly light of the sub millimeter and millimeter region through collision of electrons with the mercury atoms

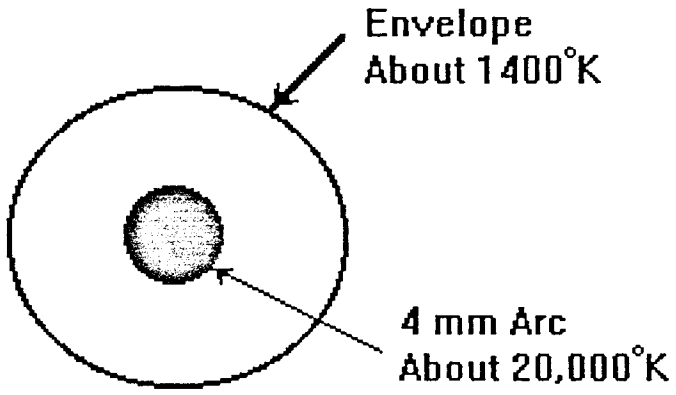

Figure 14 Cross-section of mercury lamp

The interferometer can not use more light than is transmitted through the center mirror illuminating the ring interferometer and the two mirrors at the sample area. Both systems have been designed to have f/2 optics, that is the diameter of the mirror is 1/2 of the focal length. See Figure 15.

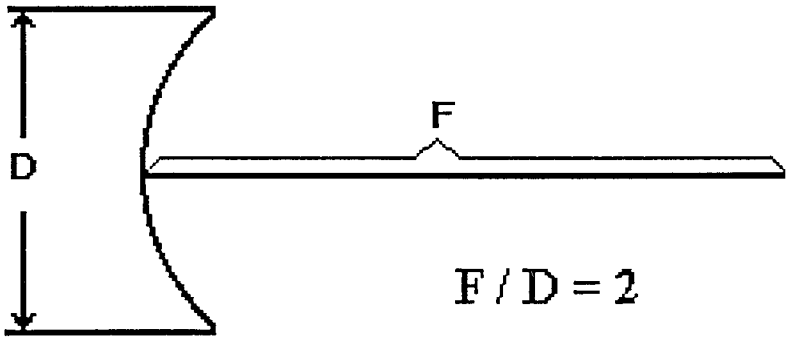

Figure 15 F/2 Optics

The total light passing through the interferometer is the product of brightness times area times solid angle. The brightness of the envelope and the arc are different. Since we are mainly interested in the long wavelength, we have to

consider the arc in the middle as the source. Our most common aperture is the diameter of the light pipe of 12 mm. We have to enlarge the diameter of the arc by a factor of 3 to fill the area of diameter of 12 mm and illuminate it with light filling f/2 optics, that is, with a total cross section angle of 30 degrees, see Figure 16.

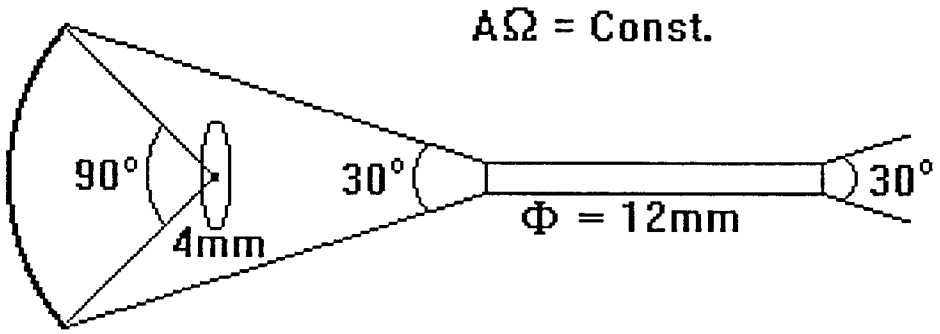

Figure 16 Using the light source efficiently. A = area; Ω = solid angle

4.3 Mirrors And Light Pipe

Mirrors are the most widely used optical elements in spectrometers. They focus, collimate, or change the direction of radiation beams. The polished surface of a mirror is coated with a highly reflecting thin layer of metal. In earlier days metal were deposited chemically, but at present vacuum-evaporation techniques are used almost exclusively. The metal chosen for infrared mirrors is usually aluminum. Aluminum has a reflectivity that is satisfactory for most purposes, and because of the hard, transparent oxide coating that forms on the aluminum surface, the quality of an aluminized mirror remains good over a long period of time. In the experiment, all the mirrors, the large focusing mirror, small reflecting mirror I, II and light source mirror, were made from this kind of first surface mirror.

A light pipe is a special kind of mirror. If the inner surface of a tube is well polished and highly reflecting, a beam of radiation can be propagated through the tube with little loss, even when the beam is diverging. This is easily understood by considering Figure 17. The beam leaving the exit end of the tube diverges at the

same rate as the initial beam. The exit opening of the tube is uniformly illuminated. The original source cannot be reimaged. On the other hand, it is often an advantage in infrared spectrometers to scramble the image before introducing it to the detector.

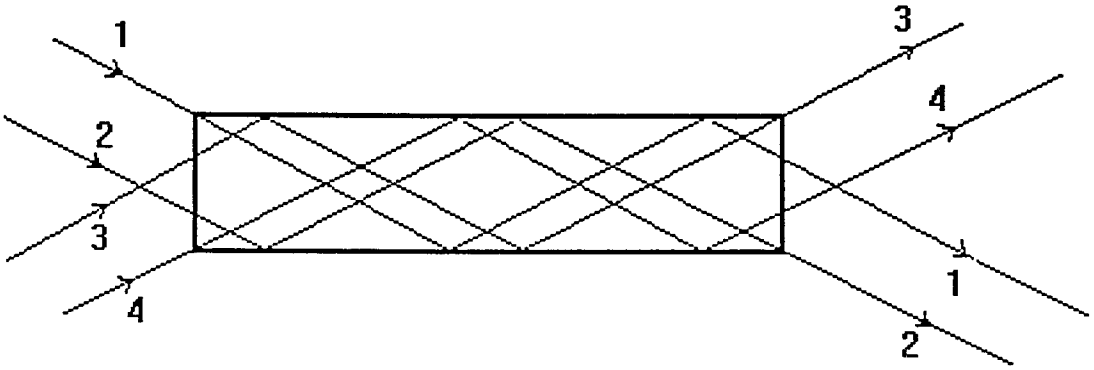

Figure 17 Diagram of the light pipe

4.4 Vacuum System

It was well known that the earth's atmosphere has a marked attenuating effect on radiation with wavelength between about 14 and 1000μm mainly due to water vapor. In far-infrared spectroscopy, one way to eliminate the absorption of water vapor could be filling the tanks with dry nitrogen or dry air, but the water vapor can not readily be reduced to a level so that it does not show up in the spectra. However, this problem can be eliminated by using a low or medium vacuum. In our experiment, it was found that a pressure of 0.5 mmHg was sufficiently low to do far-infrared spectroscopy. A well working mechanical pump is adequate for this purpose. For working under vacuum, the lamp, the chopper and the step motor of the ring interferometer need electrical feedthroughs. Since the vacuum is not high, it is possible to use simple commercial feedthroughs or make the feedthroughs themselves. In this experiment, only the power line of the chopper was "home made", by using epoxy to glue three screws on a glass flange.

For separating the spectrometer and the sample chamber, a polyethylene window was made. The design is shown in Figure 18 . For the actual operation , the use of the window permits a change of sample without loss of vacuum in the spectrometer tank.

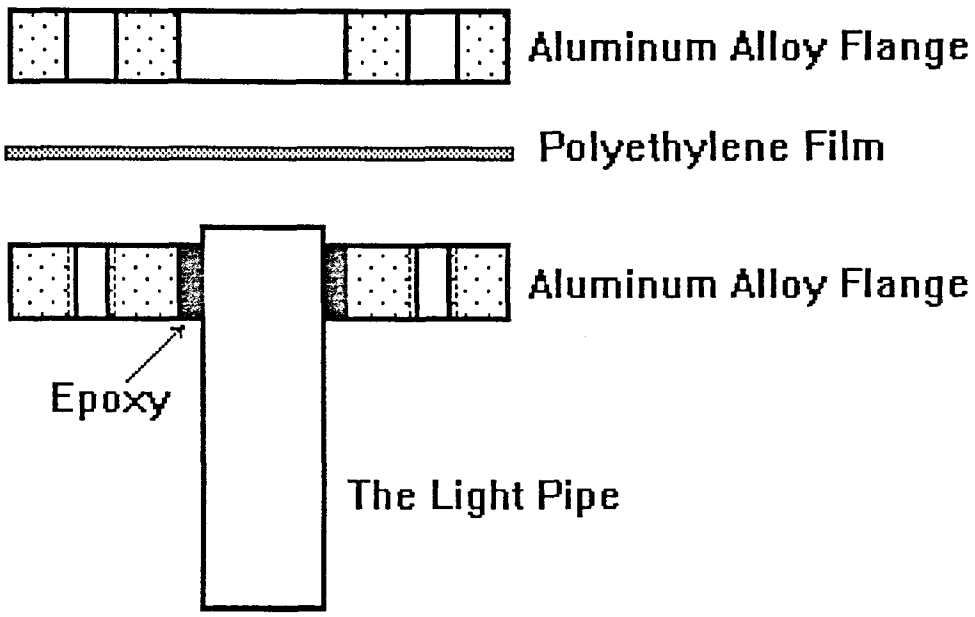

Figure 18 The schematic of polyethylene window

CHAPTER 5

DETECTION SYSTEM

5.1 Data Acquisition and Control System

Figure 19 shows the schematic of the data acquisition and step motor control system. The chopper signal is fed to the lock-in amplifier as reference signal. The white box transforms the analog output of the amplifier into a digital signal and then transmits it to the microcomputer. After reading the signal at one mirror position, the computer sends a command to move the step motor of the ring interferometer through the white box and to the stepping motor driver. When the mirror set is at its new position, the data are taken and the cycle starts again.

The IBM-PC 286 is sufficient for this purpose since for one interferogram there are not many data to be collected and the speed is low. The computer program for the task is written in gwbasic and shown in Appendix I.

5.2 Description Of Instruments For Data Acquisition And Control System

5.2.1 The White Box

Essentially an intelligent A/D converter, the OMEGA WB-31 (the "white box") is designed to interface with instruments possessing an analog output and computers with a serial communication port. Two analog input channels are provided with a standard full scale input range of plus or minus five volts and resolution of one millivolt. Normal operation requires commands to be sent over the serial link by the main computer with the interface responding with data when the commands are executed.

In the experiment, since the step motor driver needs 65 mA working current in remote mode and each digital output of the box is only capable of sinking 40

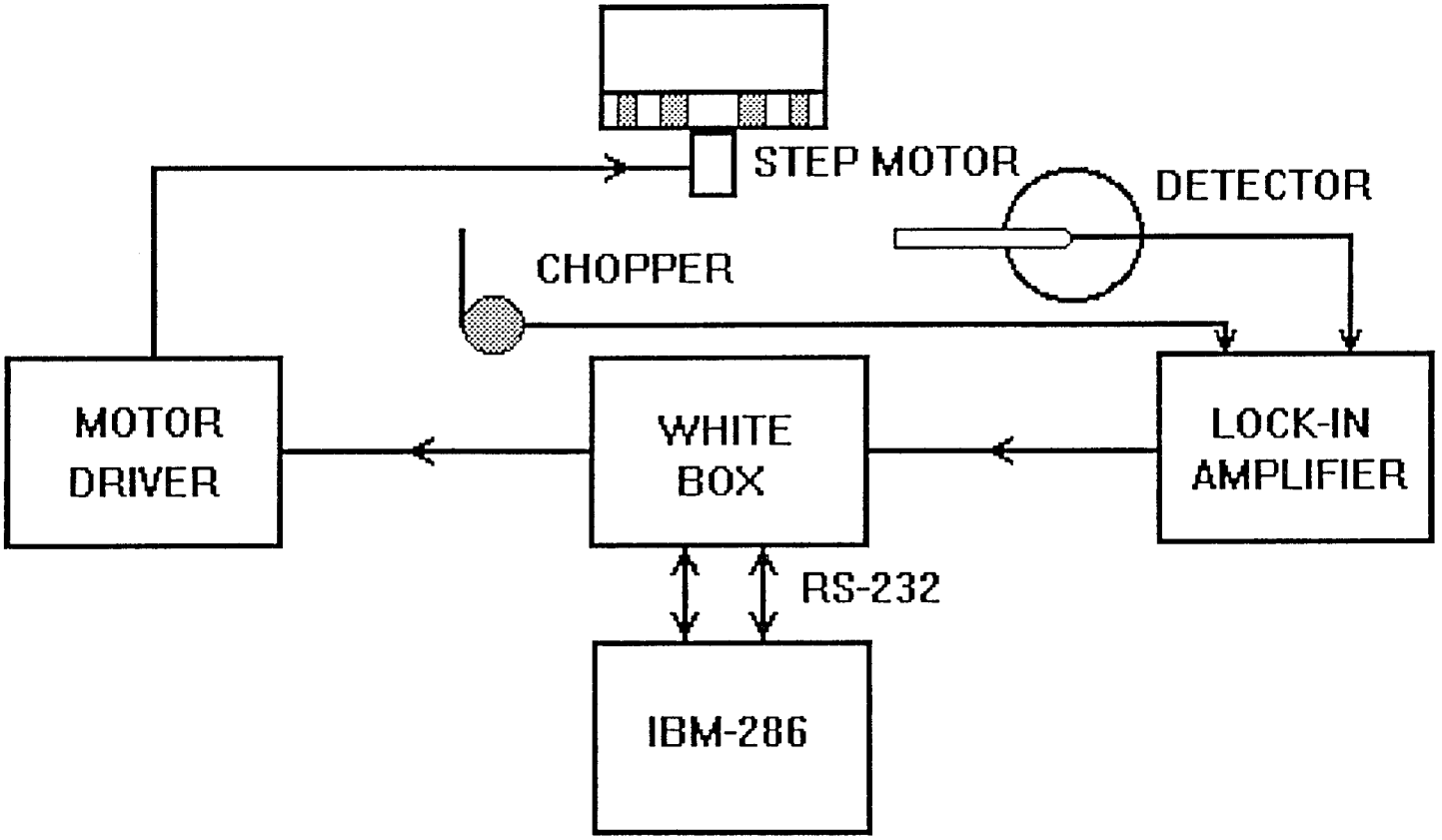

Figure 19 Data acquisition and control system

mA , a simple interface is used and shown in Figure 20. The control command Onnnn to the white box changes the function such that "0" causes the output to open and "1" causes the output to sink the current.

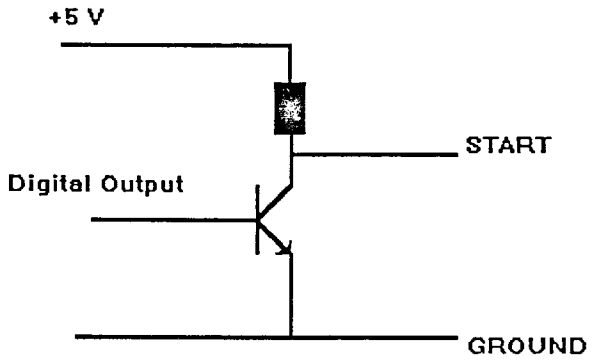

Figure 20 A simple interface for controlling the step motor driver

5.2.2 Lock-in Amplifier

The Princeton Applied Research Model 128A Lock-In Amplifier enables the accurate measurement of signals contaminated by broad-band noise, power line pickup, frequency drift, or other sources of interference. It does this by means of an extremely narrow band detector which has the center of its passband locked to the frequency of the signal to be measured. Because of the frequency lockin and narrow bandwidth, large improvements in signal-to-noise ratio can be achieved, allowing the signal of interest to be accurately measured, even in situations where it is completely masked by noise.

At the phase sensitive detector, the signal is compared with the reference signal derived from the chopper. Only those signal components which are synchronous with the reference yield a net dc detector output. Noise and other non-synchronous signals do not contribute a net dc out put, but only ac fluctuations which can be reduced to any arbitrary value according to the amount of filtering selected with the time constant switch.

5.2.3 Stepping Motor Drive System

The USM Series 100 Electronic Systems contain circuitry for driving a number of different types of stepping motors. These controllers are intended primarily for Responsyn motors but they can be used effectively to drive a wide range of other four-coil and eight-coil steppers. Since the step motor used in the ring interferometer is a four-coil Responsyn motor, the only problem remained is to control the driver by the computer.

In the experiment, due to the white box used, the driver is controlled by buffered signals. In the remote mode, the preset index can be functioned by putting START (input 2 in Figure 21) of the buffered signal connector into ground.

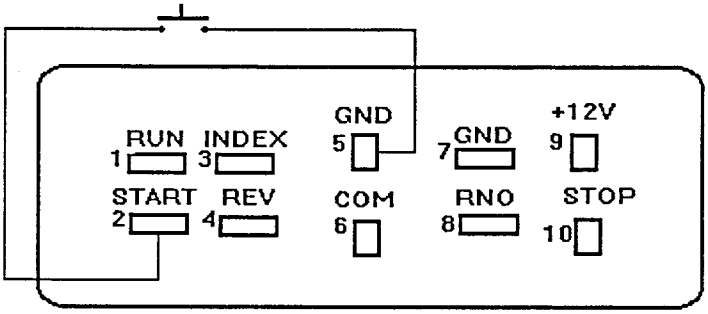

Figure 21 Buffered signal connector of step motor driver

5.3 Pyroelectric Detector

Pyroelectric detection of radiation takes place in the following manner: Radiation is absorbed and converted into heat, which increases the temperature of the crystal. The change in temperature alters the lattice spacing within the crystal, producing a change in the spontaneous electric polarization that already exists below the Curie temperature. If electrodes are applied to the crystal surfaces normal to the axis of this polarization and are connected through an external circuit, a current is generated to balance the polarization effects. This current is proportional to the

rate of change of temperature. A circuit transforms the current into a low impedance voltage (50 Ω output impedance). This voltage can be amplified again by lock-in amplifier and recorded by a computer.

Before using the liquid helium detector to get an interferogram, a pyroelectric detector was used for testing the spectrometer alignment and the function of data acquisition and control system. A signal about 40 μV was found in lock-in amplifier by putting the detector in front of the polyethylene window at spectrometer tank. Unfortunately there was no interferogram can be registered. By putting black polyethylene and black garbage bag before the detector as filter, the signal just decrease linearly. This result showed that the pyroelectric detector would not suit for the frequency range we are interested.

5.4 He - Cooled Dip - Stick Detector

A "home made" He-cooled detector, constructed by K. D. Möeller several years ago, was used in the experiment as shown in Figure 22. The detector element is mounted at the end of the second light pipe. The light from the spectrometer enters the first light pipe, is reflected by the corner mirror and then conducted by the second light pipe to the detector arrangement.

The detector is a bolometer element working with an alternating light source provided by the chopper. A 25 microns thick sapphire plate is used, covered on one side with 500 A of Sn. On the insulated side of the sapphire plate, a Ga doped germanium chip is mounted as thermometer, and 25 microns diameter brass wires are soldered on both sides of the Ge chip. One side is connected to the battery, the other side to ground and acts as heat sink. . During the "on" cycle, the light is absorbed by the Sn-film and the heat is conducted to the thermometer. The heated thermometer shows an decrease of the resistivity and the voltage from the point on the battery side of the detector element to ground is increasing. When the chopper

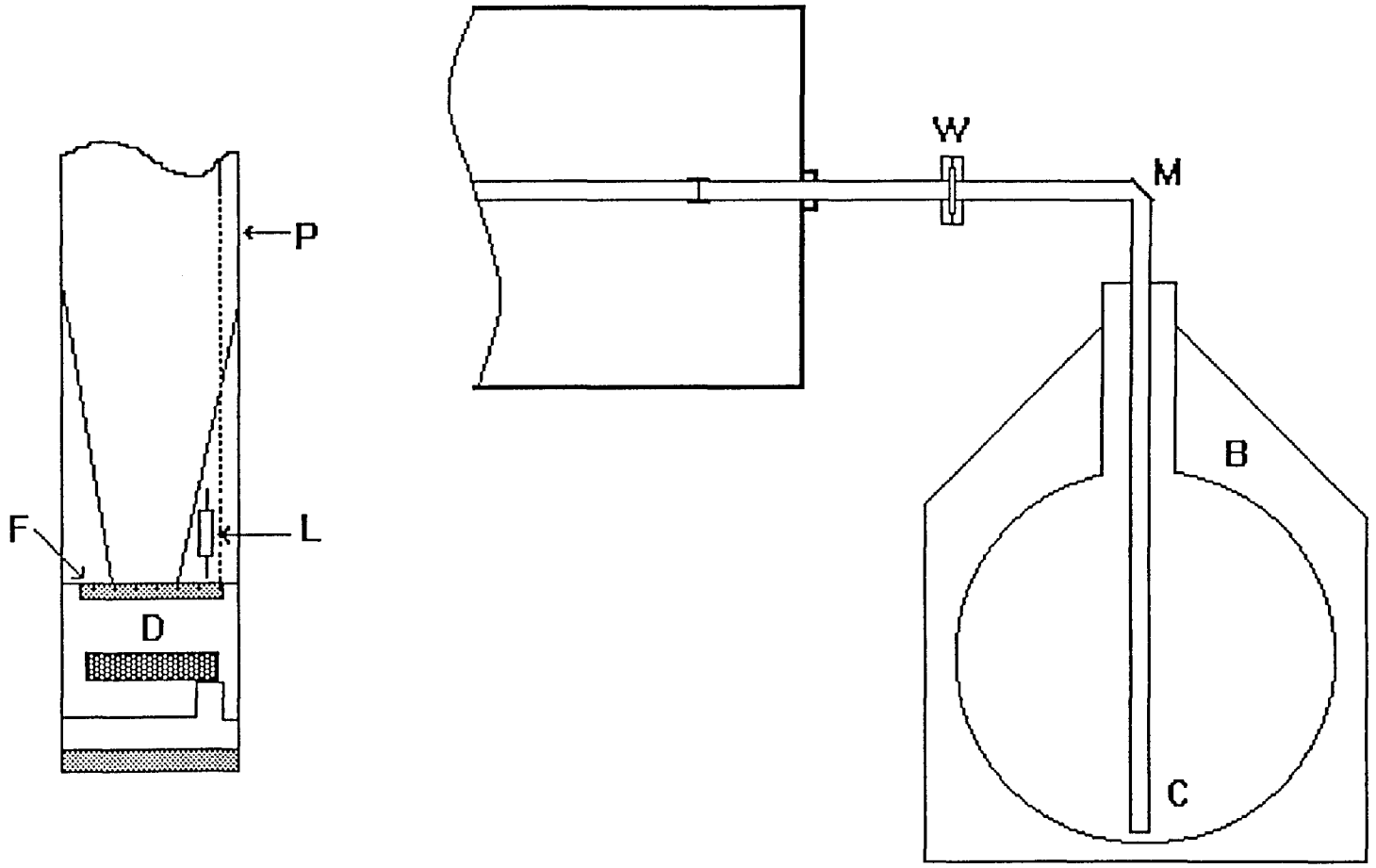

Figure 22 He-cooled dip-stick; F, filter; D, detector crystal; L, load resistor, P, pipe for wires; B, He storage Dewar; C, detector element; W, window and flanges.

is in the "off" cycle, no light is absorbed, the heat is continuously conducted to the He cooled heat sink, and the resistance of the germanium chip increases, and as a consequence the voltage from the point on the battery side decreases, for a schematic see Figure 23.

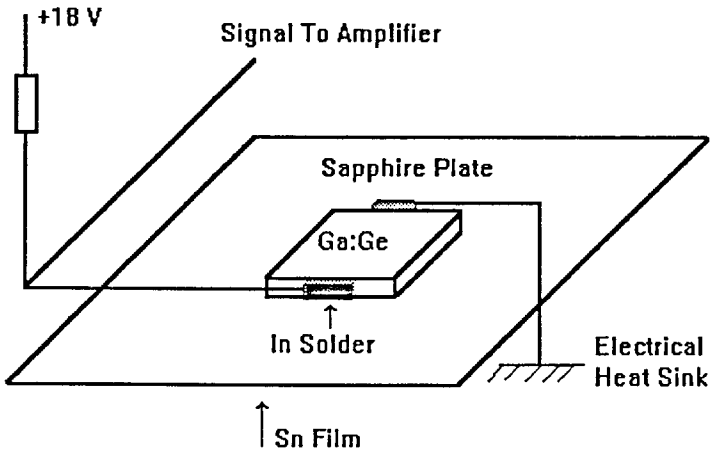

Figure 23 The schematic of detector element

The chopper frequency must not be chosen too large, so that the energy absorbed by the "on" cycle is sufficiently dissipated in the "off" cycle, typical speeds are in the 10 to 50 cycle range. The Ga:Ge element has a size of .5 mm by .5 mm by 2 mm and has a resistance at room temperature of 35 Ohm. At liquid He temperature, the resistance may be 500 000 Ohm, resulting in a high impedance input. The detection system uses a reference signal from the chopper and a lock-in amplifier. Typical settings in a far infrared spectrometer using a 250 Watt mercury lamp are settings of 25 micro Volt for the signal level.

CHAPTER 6

EXPERIMENTAL RESULTS AND CONCLUSIONS

6.1 The Interferogram

As shown in chapter 2, the interferogram is not taken as a continuous function but in steps and the sampling theorem of information theory requires that two points per cycle are taken of the highest frequency to be studied. Considering the filters in the detector, we have chosen a sampling interval of 20 steps of the step motor, corresponding to 25 microns of the mirror sets and an optical path difference of 50 microns because of reflection. The highest frequency is then

$$\nu_m = 1 / (2 \times 50 \mu m) = 100 \text{ cm}^{-1}$$

For using the fast Fourier transformation one needs 2^M points as input data. We have chosen M = 7, that is an interferogram with 128 points.

To have a good base line of the spectrum, it is recommended that one take a double sided interferogram. Since it is difficult to start the recording of the interferogram exactly at 64 points before the maximum, we have taken 7 points more on each side and have the computer program later select the interferogram with 64 points on each side of the maximum. The procedure for data recording is to go to the maximum and go back 71 points and then start the recording of 142 points.

In Figure 24 the first two interferograms we recorded are shown. These interferograms were the results by using an aperture on the second light pipe of about 9 mm in diameter. The intensity in the diagram is the data read from the lock-in amplifier which is adjusted in: sensitivity with 2.5 μV, zero off set 0.4 and time constant 3 seconds. The data representing interferogram points are collected in a file and can be easily read into the Fourier transform program.

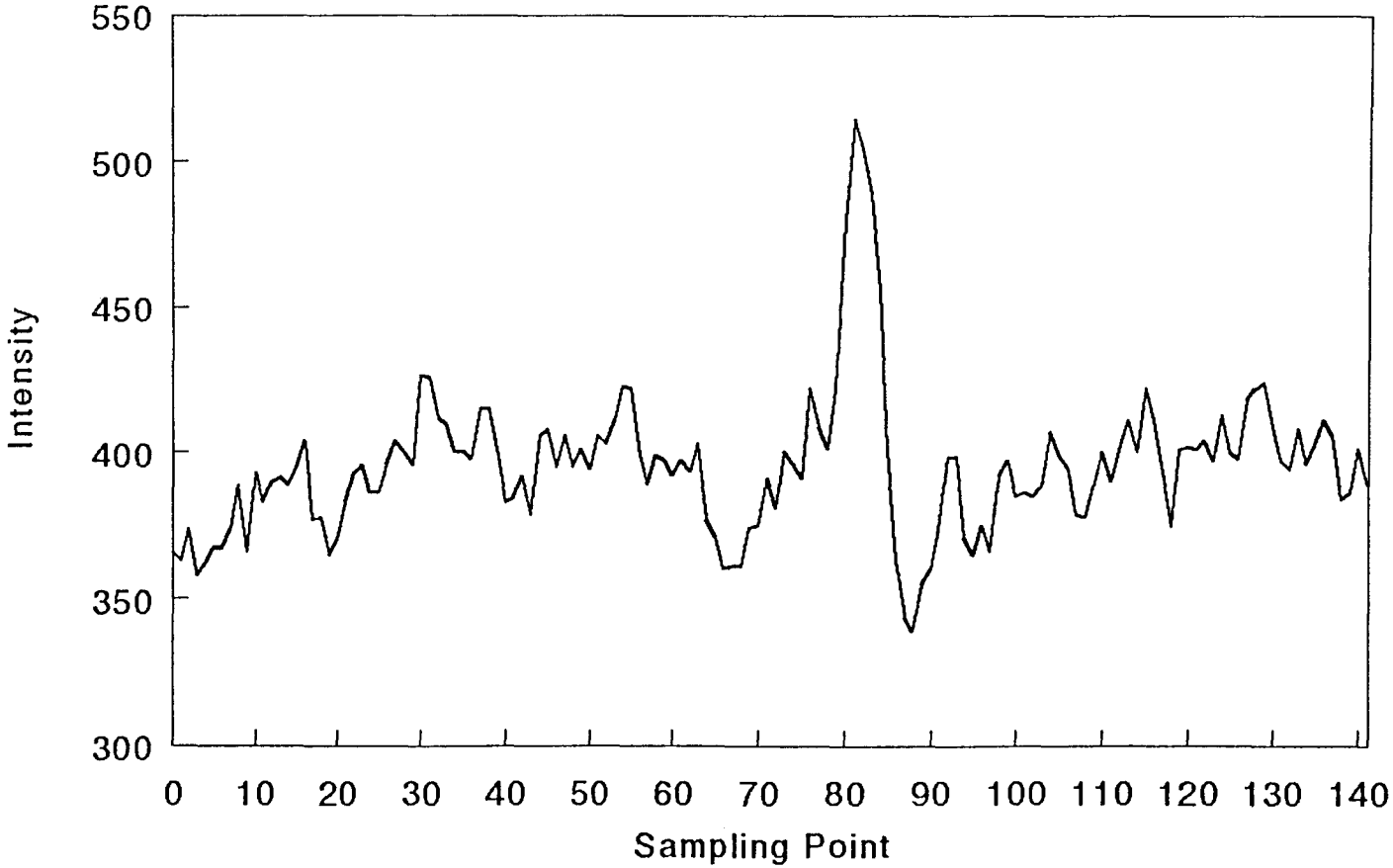

Figure 24 (a) Interferogram QT2

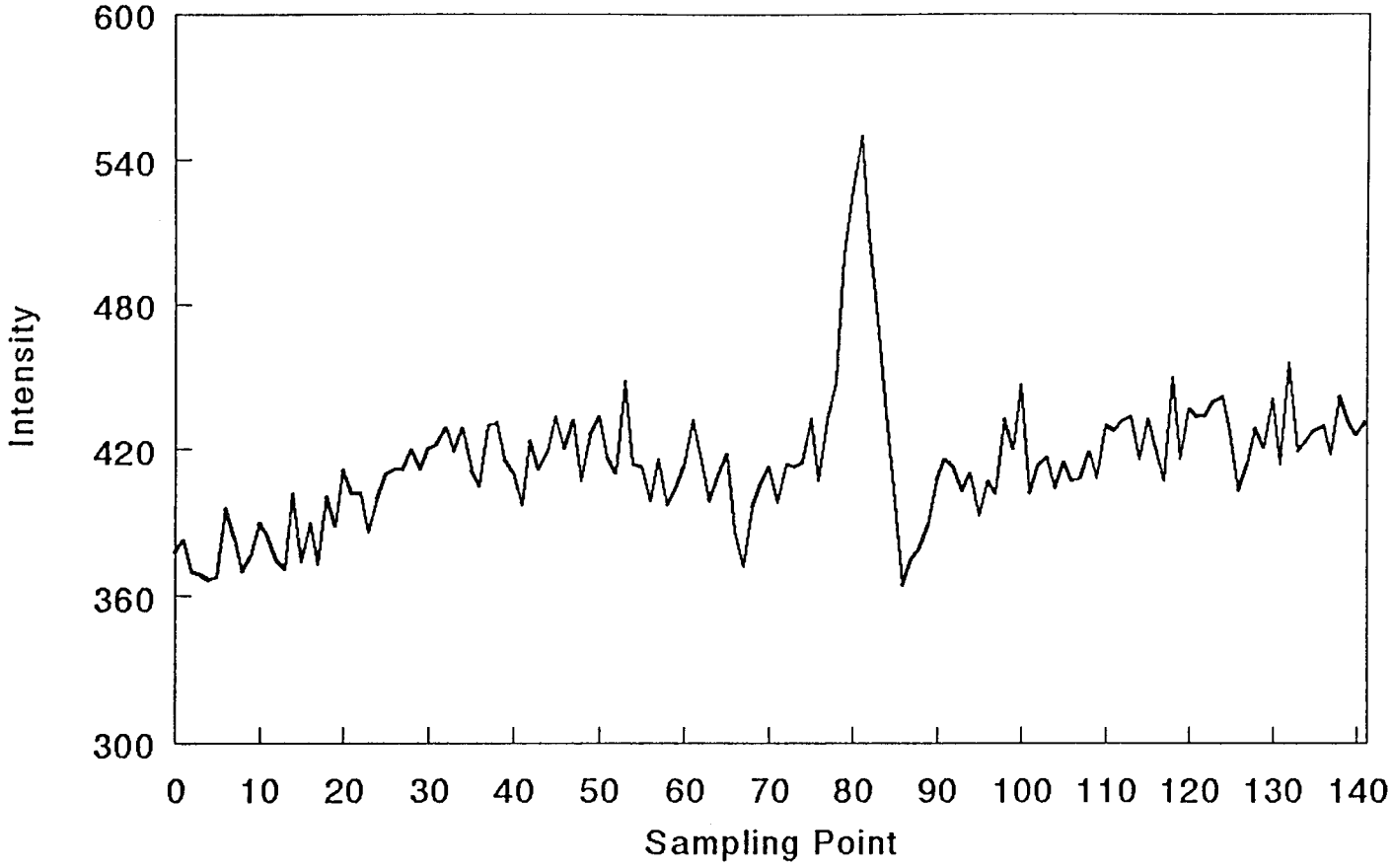

Figure 24 (b) Interferogram QT26

6.2 The Spectra

The Fourier transform program we used to get the spectra is shown in Appendix II. At first, the program prepares the data for input to the Fourier transformation algorithm. It selects the maximum point, counts to both sides to the 64th point and defines a new series A(n) of 128 points.

The interferogram function corresponding to the spectrum of frequencies we want to study is obtained by subtracting the background we have in the measured data. To do this, an average is taken of the points in the arrangement A(n), for n = 1 to 10 and n = 118 to 128. A line is defined through these two average points and the value of the line for all 128 points is subtracted from A(n) resulting in a new series of points B(n).

This program needs the input data rearranged so that the maximum points are points 1 and 128. Therefore, the maximum point of number 64 is assigned as first point and half the interferogram to point 128 is assigned as points 2 to 64. The first point in series B(n) is assigned to point 65 and the maximum point is now the last point, that is 128. This is the series C(n) which is the input to the Fourier transform algorithm. For more details of the Cooley-Turkey algorithm which is used in this program, see reference 9.

Since we have used a double sided interferogram, the Fourier transformation results in a double spectrum. The double sided interferogram had 128 points, and therefore the spectrum is a spectrum of 64 frequency intervals. The length of each of the frequency intervals has the value of the maximum frequency divided by 64, where the maximum frequency is determined by the cosine sampling interval, that is

$$\nu_m = 1/2\,l\,.$$

The sampling interval is as well related to the length of the interferogram 2L by

$$l = 2L/128\,.$$

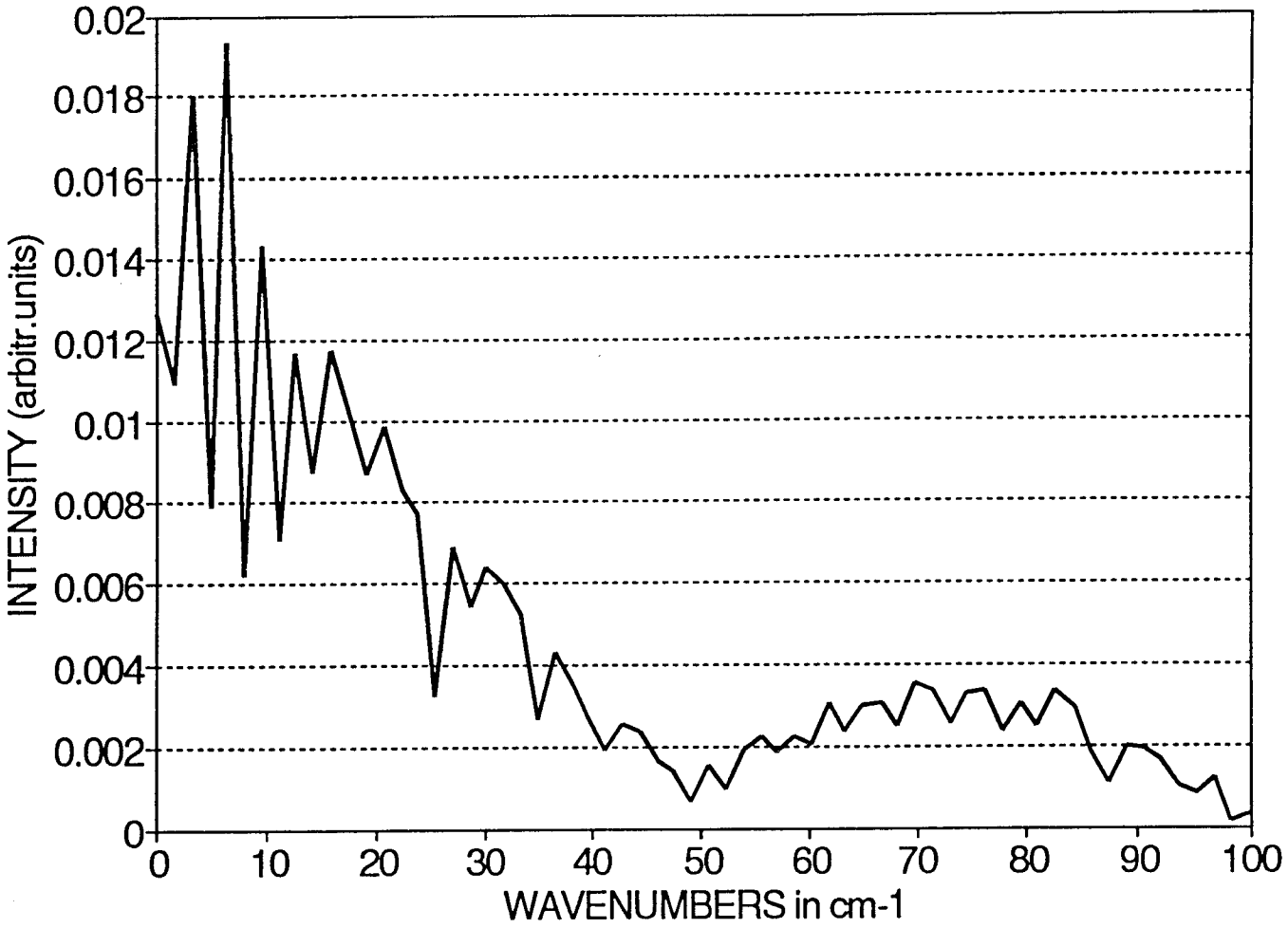

Figure 26 (a) Spectra tqt2

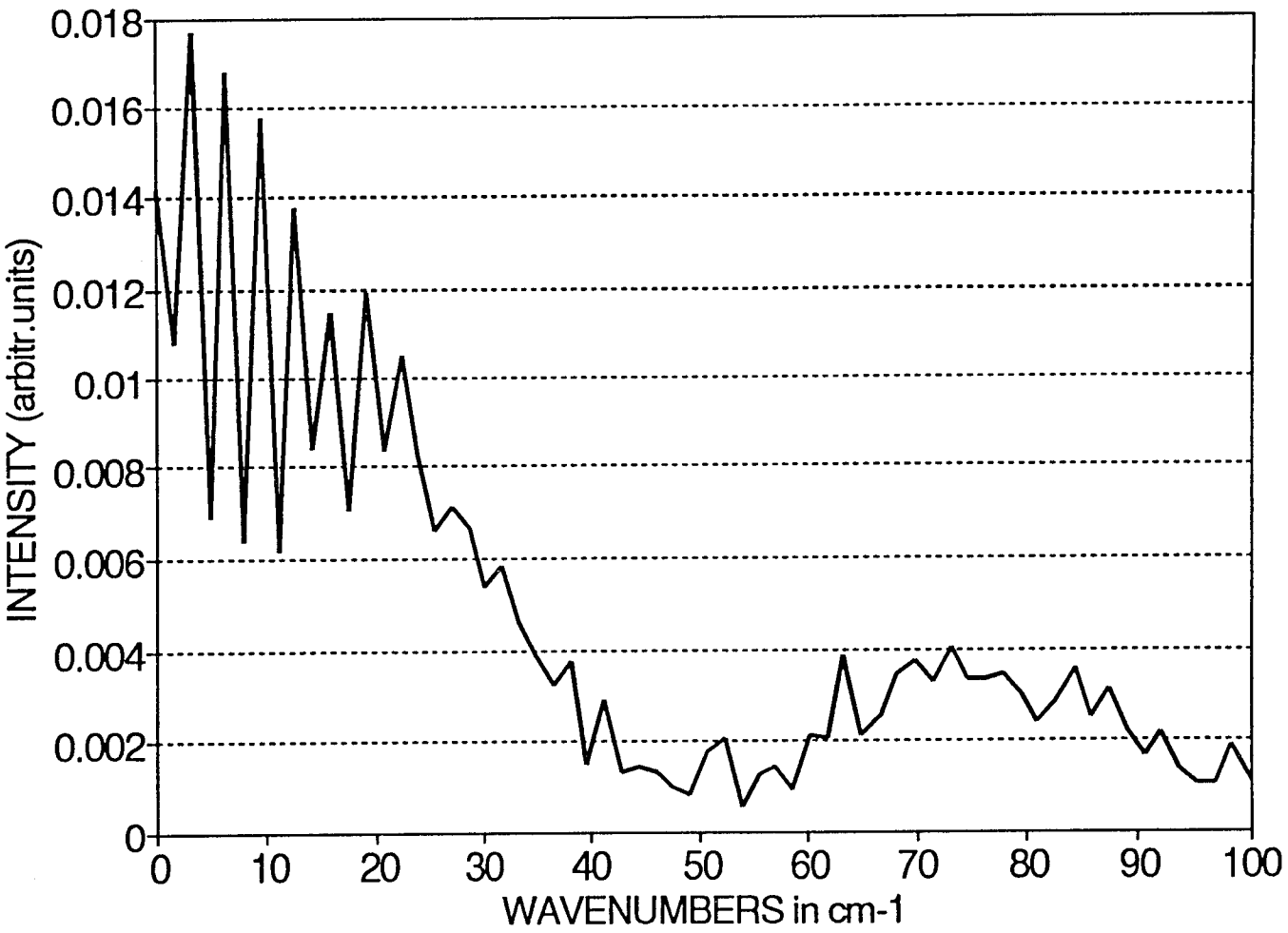

Figure 25 (b) Spectra tqt26

The resolving power is in our case 64 and the resolution is $\Delta\nu = \nu_m/64$ or 1/2L. The spectra obtained from the interferogram of Figure 24 are shown in Figure 25.

6.3 Absorption of Polyethylene and Fringe Pattern.

The two spectra are very similar. The strong absorption of the polyethylene window of the detector appears at 50 cm^{-1}. The fringes at the low frequency end of the spectrum are probably fringes from the quartz window sealing the He-cooled detector on the high temperature side. We can make an estimate of the thickness d using the formula

$$d = 1/(2\, n\, \Delta\nu)\,,$$

where n is the refractive index, in our case of quartz about 1.5, and $\Delta\nu$ the width of the fringes, in our case around 4 cm^{-1}. Since $\Delta\nu$ is not very accurate, we obtain for d the approximate value of 1 mm, about the value of the window.

6.4 Conclusions

Our ring interferometer--a wavefront dividing vacuum interferometer which use two interpenetrating sets of reflectors has been constructed and developed to operation condition.

The interferometer has center symmetric reflectors instead of parallel reflectors as used by the lamellar grating. The advantage of the center symmetric arrangement will be to use large apertures resulting in a large throughput compared to the lamellar grating. This advantage could not be studied yet. The obtained spectra show the absorption of a polyethylene filter at 50 cm^{-1} of the detector and fringes at the long wavelength rang of a thin quartz window of thickness 1 mm.

APPENDIX I

DATA ACQUISITION AND CONTROL PROGRAM

```
10 CLS
20 CLEAR ,,1024
30 DIM SMPL(142), SA(50)
40 PRINT "CHOICE: (1) Aquire new spectrum; (2) Plot old; (3) Stop"
50 INPUT CHOICE
60 IF CHOICE =1 THEN GOSUB 100
70 IF CHOICE = 2 THEN GOSUB 4000
80 IF CHOICE = 3 THEN GOTO 430
90 GOTO 40
100 REM prompt for name of file to store data in.
110 INPUT "Filename for Data  ";F$
120 REM check for good name
130 IF F$="" THEN PRINT "You must enter a filename!!":GOTO 110
140 REM add extent if necessary
150 IF INSTR(1,F$,".")=0 THEN F$=F$+".prn"
160 REM how many samples
170 INPUT "how many points ";S%
180 IF S%<=0 THEN PRINT "At least one sample, please!":GOTO 170
190 REM settling time
200 INPUT "How long to wait between samples ";D%
210 IF D%<=0 THEN PRINT "Must be >0! ":GOTO 200
220 REM
230 REM white box params: com1:, 1200bd, 7 data, 1 stop, no parity
240 OPEN "com1:1200,N,7,1,CS,DS,RS" AS #1
250 PRINT #1, "S9"
260 REM
270 REM
280 SCREEN 2: CLS
290 FOR SMPLCNT = 1 TO S%
300 GOSUB1080: REM TAKE SAMPLE
310 SMPL(SMPLCNT) = SAMPLE
320 GOSUB 2000
330 GOSUB 1000
340 NEXT SMPLCNT
350 REM
```

```
360 REM store all data on disk
370 CLOSE #1: OPEN F$ FOR OUTPUT AS #1
380 FOR SMPLCNT =1 TO S%
390 PRINT #1, SMPLCNT,SMPL(SMPLCNT),0
400 NEXT SMPLCNT
410 CLOSE #1
420 BEEP:BEEP:REM beep to show all done
430 LOCATE 1,1
440 END
1000 REM
1010 REM
1020 PRINT #1, "OXX1X": REM MOVE MOTER
1030 TD% = 1: GOSUB 3000: REM WAITE 1 SEC.
1040 PRINT #1, "OXX0X"
1050 TD%=D%:REM wait preset time for settling
1060 GOSUB 3000
1070 RETURN
1080 REM
1090 FOR K = 1 TO 50
1100 PRINT #1, "C":PRINT #1, "E":REM take sample
1110 WHILE LOC(1) <> 9
1120 WEND
1130 D$ = INPUT$ (LOC(1), 1): REM READ INPUT
1140 SA(K) = VAL(D$)
1150 NEXT K
1160 SAMPLE1 = 0
1170 FOR I = 1 TO 50
1180 SAMPLE1 = SAMPLE1 + SA(I)
1190 NEXT I
1200 SAMPLE = SAMPLE1 / 50
1210 RETURN
1220 REM wait for sample ready
1230 REM
2000 REM plot the data on screen 2
2010 IY = SMPLCNT * 600 / S%: IX = 160 - SAMPLE * 160
2020 LINE (IY,IX) - (IY,IX)
2030 IF SMPLCNT = S% THEN LINE (0,150) -(600,150): LINE (300,0) -
(300,160)
2040 RETURN
3000 REM delay d% seconds
3010 FOR TDC=1 TO D%
3020 FOR TDC1=1 TO 5000:NEXT
```

```
3030 NEXT
3040 RETURN
4000 REM load & plot a file
4010 INPUT "file name to plot ";F$
4020 INPUT "FILE POINT NUMBER?";S%
4030 CLS
4040 OPEN F$ FOR INPUT AS #1
4050 FOR J = 1 TO S%
4060 INPUT #1, SMPLCNT, SMPL(J), K
4070 SAMPLE = SMPL(J)
4080 GOSUB 2000
4090 NEXT J
4100 CLOSE #1
4110 LOCATE 1,1
4120 RETURN
```

APPENDIX II

FOURIER TRANSFORM PROGRAM

```
10 PRINT  "FFT/IFT"
20 PRINT "***********"
30 INPUT "DATE";DA$
40 INPUT "HR";HR$
50 INPUT "FWD-DR-INV";AN$
60 IF AN$="F" THEN  D=0
70 IF AN$="I" THEN  D=1
80 INPUT "M=";M
90 N=2^M
100 PRINT "N=";N
110 DIM X(2*N+20,2)
120 DIM C(2*N+30)
130 DIM CC(2*N+30)
140 DIM B(2*N+30)
150 DIM A(N+20)
160 IF D=0 THEN PRINT "INPUT  TIME DOMAIN DATA"
170 IF D=1 THEN  PRINT"INPUT  FREQ DOMAIN DATA"
180 PRINT "ENTER [*.PRN]"
190 LINE INPUT F$
200 OPEN F$ FOR INPUT AS #1
210 FOR G=1 TO N+14 STEP 1
220 INPUT #1,JUNK,C(G),A
230 NEXT G
240 FOR G=1 TO N+14
250 Z=C(1)+C(2)+C(3)+C(4)+C(5)+C(6)+C(7)+C(8)+C(9)+C(10)
260 U=C(N+5)+C(N+6)+C(N+7)+C(N+8)+C(N+9)+
        C(N+10)+C(N+11)+C(N+12)+C(N+13)+C(N+14)
270 ZZ=(Z-U)/(10*(N+14-10))
280 CC(G)=C(G)+ZZ*G
290 NEXT G
300 MAX=0
310 MAXIND=0
320 FOR I=1 TO N+14
330 IF CC(I)>MAX THEN MAX=CC(I): MAXIND=I
340 NEXT I
```

```
350 PRINT CC(MAXIND)
360 LET P=MAXIND
361 PRINT P
370 FOR G=1 TO N
380 LET B(G)=CC(P-(N/2)+G)
390 NEXT G
400 FOR G=1 TO N
410 LET V=(B(1)+B(2)+B(3)+B(4)+B(5)+B(6))/6
420 LET W=(B(N)+B(N-1)+B(N-2)+B(N-3)+B(N-4)+B(N-5)+B(N-6))/6
430 H=(V+W)/2
440 A(G)=B(G)-H
450 NEXT G
460 FOR G=1 TO N/2
470 X(G,0)=A((N/2)+G)
471 X(G,1)=0
480 NEXT G
481 FOR G=1 TO 5
483 NEXT G
490 FOR G=(N/2)+1 TO N
500 X(G,0)=A(G-(N/2))
510 X(G,1)=0
520 NEXT G
521 FOR G=N-5 TO N
523 NEXT G
530 CLOSE 1 : OPEN "O",#2,"FTIN5.PRN"
540 FOR G=1 TO N STEP 1
550 PRINT #2,;G;" ";X(G,0);" ";X(G,1)
560 NEXT G
570 GOSUB 1230
580 PRINT "///////"
590 IF D=0 THEN  PRINT "NOW IN FREQ DOMAIN"
600 DIM XX(2*N+20,2)
610 PRINT "XFRMD DATA IS:"
620 PRINT "POINT   REAL    IMAG"
630 PRINT "ENTER OUTPUT [*.PRN]"
640 LINE INPUT G$
660 PRINT
670 PRINT
680 PRINT
700 CLOSE 2 : OPEN G$ FOR OUTPUT AS #3
710 DIM R(N)
720 DIM RR(N)
```

```
730 FOR I=1 TO N/2 STEP 1
740 XX(I,0)=X(N/2+I,0)
750 XX(I,1)=X(N/2+I,1)
760 LET R(I)=((XX(I,0))^2+(XX(I,1))^2)
770 LET RR(I)=SQR(R(I))
780 PRINT #3,;I;"  ";XX(I,0);" ";XX(I,1);" ";RR(I)
790 NEXT I
800 FOR I=(N/2)+1 TO N STEP 1
810 XX(I,0)=X(I-(N/2),0)
820 XX(I,1)=X(I-(N/2),1)
830 LET R(I)=((XX(I,0))^2+(XX(I,1))^2)
840 LET RR(I)=SQR(R(I))
850 PRINT #3,;I;"  ";XX(I,0);" ";XX(I,1);" ";RR(I)
860 NEXT I
870 MAX=0
880 MAXIND=0
890 FOR J=1 TO N/2
900 IF RR(J)>MAX THEN MAX=RR(J): MAXIND=J
910 NEXT J
920 PRINT RR(MAXIND)
930 DEFINT K
940 DIM K(N)
950 FOR I=1 TO (N/2)
960 LET K(I)=(65*RR(I)/(RR(MAXIND)))
970 DEFINT K
980 NEXT I
990 PRINT "INPUT HIFR"
1000 INPUT HIFR
1010 FOR I=1 TO (N/2)
1020 LET F=I*HIFR/(N/2)
1030 PRINT
1050 FOR Z=0 TO 70
1060 IF Z<>0 THEN 1120
1070 PRINT (HIFR-F);
1090 GOTO 1100
1100 IF K(I)>0 THEN 1150
1110 GOTO 1180
1120 IF Z=K(I) THEN 1160
1130 PRINT " ";
1150 NEXT Z
1160 PRINT I;"*";
1180 NEXT I
```

```
1190 PRINT
1200 PRINT "========"
1210 PRINT "  -DONE-    "
1220 END
1230 REM**********************
1240 REM   FFT/IFT  SUBROUTINE
1250 REM**********************
1260 N=2^M
1270 REM**** DO BIT SHUFFLE***
1280 N2=N/2
1290 N1=N-1
1300 J=1
1310 FOR I=1 TO N1
1320 IF I>=J THEN 1390
1330 T1=X(J,0)
1340 T2=X(J,1)
1350 X(J,0)=X(I,0)
1360 X(J,1)=X(I,1)
1370 X(I,0)=T1
1380 X(I,1)=T2
1390 K=N2
1400 IF K>=J THEN 1440
1410 J=J-K
1420 K=K/2
1430 GOTO 1400
1440 J=J+K
1450 NEXT I
1460 REM*****END OF SHUFFLE*******
1470 S1=-1
1480 IF D=0 THEN 1500
1490 S1=1
1500 P1=3.1415926535898#
1510 FOR L=1 TO M
1520 L1=2^L
1530 L2=L1/2
1540 U1=1
1550 U2=0
1560 W1=COS(P1/L2)
1570 W2=S1*SIN(P1/L2)
1580 FOR J=1 TO L2
1590 FOR I=J TO N STEP L1
1600 I1=I+L2
```

```
1610 REM***DO BUTTERFLY*****
1620 V1=(X(I1,0)*U1-X(I1,1)*U2)
1630 V2=(X(I1,1)*U1+X(I1,0)*U2)
1640 X(I1,0)=X(I,0)-V1
1650 X(I1,1)=X(I,1)-V2
1660 X(I,0)=X(I,0)+V1
1670 X(I,1)=X(I,1)+V2
1680 NEXT I
1690 REM********DO TWIDL FACTOR ********
1700 U3=U1
1710 U4=U2
1720 U1=(U3*W1-U4*W2)
1730 U2=(U4*W1+U3*W2)
1740 NEXT J
1750 NEXT L
1760 IF D=1 THEN  1810
1770 FOR  I=1 TO N
1780 X(I,0)=X(I,0)/N
1790 X(I,1)=X(I,1)/N
1800 NEXT I
1810 RETURN
```

REFERENCES

1. Möller, Karl Dieter and Rothschild, Walter G. *Far - Infrared Spectroscopy.* New York: Wiley-Interscience. (1971)

2. Robinson, L.C. *Physical Principles of Far-Infrared Radiation.* .New York and London: Academic Press. (1973)

3. Finch, Arthur, P. N. Gates, K. Padiffe, F.N. Dickson and F. F. Bentley. *Chemical Application of Far Infrared Spectroscopy* . London and New York: Academic Press. (1970)

4. Willeams, Dudley . *Spectroscopy.* New York: Academic Press.(1970)

5. Stewart, James E. *Infrared Spectroscopy.* New York: INC. (1970)

6. Möller, K.D. *Optics.* California: Mill Valley.(1988)

7. Möller, K.D. "Wavefront Dividing Interferometers". *Infrared Physics.* 32 (1991): 321-311

8. Möller, K.D., D.P. Siddons and C.J. Hirschmugl. "Two-Mirror Wave - Front Dividing Interferometer for Infrared Synchrotron Radiation". *Applied Optics.* 30 (1991): 4297-4301

9. Bell, Robert John. *Introductory Fourier Transform Spectroscopy.* New York and London: Academic Press. (1972)

10. Rubens, H. and R.W. Wood. "Focal Isolation of Long Heat Waves." *Phil. Mag.* 21 (1991): 249

11. Richards, P.L. "High-resolution Fourier Transform Spectroscopy in the Far Infrared." *J. Opt. Soc. Am.* 54 (1964): 1474

12. Plyer,E.K., D.J.C. Yates, and H.A. Gebbie. "Radiant Energy from Sources in the Far Infrared." *J. Opt. Soc. Am.* 52 (1962): 859